


# CDF $W$ -boson mass and muon $g - 2$ in a type-X two-Higgs-doublet model with a Higgs-phobic light pseudoscalar

Jinheung Kim<sup>1,\*</sup>, Soojin Lee<sup>1,†</sup>, Prasenjit Sanyal<sup>2,‡</sup> and Jeonghyeon Song<sup>1,§</sup>

<sup>1</sup>*Department of Physics, Konkuk University, Seoul 05029, Republic of Korea*

<sup>2</sup>*Asia Pacific Center for Theoretical Physics, Pohang 37673, Republic of Korea*

 (Received 17 May 2022; revised 20 June 2022; accepted 12 July 2022; published 1 August 2022)

The recent measurement of the  $W$  boson mass by the CDF collaboration adds an anomaly to the longstanding discrepancy in the muon anomalous magnetic moment,  $\Delta a_\mu$ . Although type-X in the two-Higgs-doublet model provides an attractive solution to  $\Delta a_\mu$  through a light pseudoscalar  $A$ , the model confronts the exotic Higgs decays of  $h \rightarrow AA$  and the lepton flavor universality data in the  $\tau$  and  $Z$  decays. To save the model, we propose that the light pseudoscalar be Higgs-phobic. Through the random scanning over the entire parameter space, we perform a comparative study of the Higgs-phobic type-X with and without the CDF  $m_W$  measurement, called the CDF and PDG cases, respectively. Both cases can explain the two anomalies as well as all the other constraints, but have significant differences in the finally allowed parameter space. For example, a small region with almost degenerate masses of new Higgs bosons around 100 GeV is allowed only in the PDG case. The cutoff scale of the model is also studied via the analysis of renormalization group equations, which reaches up to  $10^5$  GeV ( $10^7$  GeV) in the CDF (PDG) case. Since the dominant decay modes are  $A \rightarrow \tau\tau$ ,  $H \rightarrow ZA$ , and  $H^\pm \rightarrow W^\pm A$  in most of the viable parameter space, we propose the  $4\tau + VV'$  states as the golden discovery channel at the LHC.

DOI: [10.1103/PhysRevD.106.035002](https://doi.org/10.1103/PhysRevD.106.035002)

## I. INTRODUCTION

The CDF collaboration at the Fermilab National Accelerator Laboratory has come out with the most precise measurement of  $W$  boson mass [1]

$$m_W^{\text{CDF}} = 80.4335 \pm 0.0094 \text{ GeV}, \quad (1)$$

using the dataset collected at  $8.8 \text{ fb}^{-1}$  luminosity. The new mass deviates from the Standard Model (SM) prediction of  $m_W^{\text{SM}} = 80.357 \pm 0.006 \text{ GeV}$  [2] by  $7\sigma$ . Previously the world average of  $m_W$  measurements [2] was only  $1.8\sigma$  standard deviation from  $m_W^{\text{SM}}$ . The discrepancy of the  $W$  mass still needs to be confirmed as there is a tension between the CDF measurement and ATLAS report [3]. However, if we accept the new mass of  $W$  boson then the validity of the SM is under serious question. An efficient way to parametrize the discrepancy of  $W$  boson mass is the

Peskin-Takeuchi oblique parameter ( $S$ ,  $T$ , and  $U$ ): a new physics model beyond the SM (BSM) can be explored by its contribution to the gauge boson self energies. In most models, the contribution to  $U$  is significantly small, so setting  $U = 0$  is usually accepted. Then we have large shift of the central values [4–8] such that  $S_{\text{CDF}} = 0.15 \pm 0.08$  and  $T_{\text{CDF}} = 0.27 \pm 0.06$  with the correlation  $\rho_{ST} = 0.93$  [4]. Various BSM models have been studied to explain the new oblique parameters [4,6–57].

Another long-standing problem in particle physics is the muon anomalous magnetic moment. The combined result of the Fermilab National Accelerator Laboratory experiment [58,59] and the Brookhaven National Laboratory experiment [60] has shown a deviation from the SM prediction [61–81] by  $4.2\sigma$ , which is reported to be

$$\Delta a_\mu = a_\mu^{\text{exp}} - a_\mu^{\text{SM}} = 251(59) \times 10^{-11}. \quad (2)$$

Two anomalies of  $m_W^{\text{CDF}}$  and  $\Delta a_\mu$  call for new physics. Several works have been done to simultaneously explain the two anomalies in the context of  $U(1)$  gauge extended models with vectorlike leptons [82–84], vector leptoquark model [85], scalar leptoquark model [86,87], Zee model [88], vectorlike lepton models [89,90], a flavor conserving two-Higgs-doublet model (2HDM) [91], and next-to-minimal supersymmetric model [92].

\*jinheung.kim1216@gmail.com

†soojinlee957@gmail.com

‡prasenjitsanyal@apctp.org

§jhsong@konkuk.ac.kr

Published by the American Physical Society under the terms of the [Creative Commons Attribution 4.0 International license](https://creativecommons.org/licenses/by/4.0/). Further distribution of this work must maintain attribution to the author(s) and the published article's title, journal citation, and DOI. Funded by SCOAP<sup>3</sup>.

In this paper, we study type-X (lepton-specific) 2HDM in light of the CDF  $W$  boson mass and muon  $g-2$  anomalies. Type-X has drawn a lot of interest as an explanation of  $\Delta a_\mu$  [93–104]. One of its most salient characteristics is the enhanced coupling of the BSM Higgs bosons (neutral  $CP$ -even  $H$ ,  $CP$ -odd  $A$ , and charged Higgs  $H^\pm$ ) to the leptons by  $\tan\beta$ , the ratio of the vacuum expectation values of two Higgs doublet fields. Through the enhanced leptonic coupling, type-X can explain muon  $g-2$  anomaly via two loop Barr-Zee diagram with  $\tau$ -loop [105,106]. The contributions to  $\Delta a_\mu$  can be sizable and positive with large  $\tan\beta$  and small  $M_A$ . However, a light pseudoscalar with  $M_A < m_h^{\text{SM}}/2$  opens up  $h_{\text{SM}} \rightarrow AA$  which is severely constrained by  $h_{\text{SM}} \rightarrow AA \rightarrow 4\tau/2\mu 2\tau$  channels [107]. Kinematical solution of  $M_A > m_h^{\text{SM}}/2$  demands very large  $\tan\beta$  above 100 for the explanation of  $\Delta a_\mu$ . Then this extremely large  $\tan\beta$  enhances the contributions to the lepton flavor universality (LFU) data in the  $\tau$  and  $Z$  decays, which invalidates the model [103]. This motivates us to consider the Higgs-phobic type-X where the vertex  $h$ - $A$ - $A$  vanishes.

An essential question is how the changes of  $S$  and  $T$  due to the CDF  $W$  boson mass affect the parameter space compatible with the muon  $g-2$  as well as all the theoretical and experimental constraints. To comprehensively answer the question, we will perform a scan over the entire parameter space in four steps, considering both the old and new sets of  $S$  and  $T$ . In step I, we impose the theoretical bounds (vacuum stability of the potential, unitarity, perturbativity) and the muon  $g-2$  constraint. In step II, we include the  $S$  and  $T$  parameters before and after the CDF  $m_W$  measurement. In step III, we impose the Higgs precision data and the most updated direct search bounds from the LEP, Tevatron, and LHC. In step IV, we further restrict the parameter space through the global  $\chi^2$  fit to  $\Delta a_\mu$  and the LFU data. Based on the scan results, we will find the common and different features before and after the CDF  $m_W$  measurement. Another important question is to what energy scale the finally allowed parameter points survive. We will perform the renormalization group equation (RGE) analysis to obtain the cutoff scale  $\Lambda_c$  of every viable parameter point. The final question is how to probe the Higgs-phobic type-X at the LHC. In the literature, the multi- $\tau$  states have extensively been studied for type-X,  $2\tau$  [108],  $2\mu 2\tau$  [109,110],  $b\bar{b}\tau^+\tau^-$  [111],  $3\tau$  [109,112],  $4\tau$  [109,112], and  $4\tau + V$  [112]. We will show that  $4\tau + ZW/WW$  is the golden discovery channel. These are our new contributions.

The paper is organized in the following way. In Sec. II, we give a brief review of type-X 2HDM and the characteristics of the Higgs-phobic pseudoscalar. In Sec. III, we do the parameter scanning for both old and new sets of  $S$  and  $T$  values. In Sec. IV, we study the RGE evolutions and the cutoff scales. Section V deals with the LHC

phenomenology of the Higgs-phobic type-X. Finally we conclude in Sec. VI.

## II. TYPE-X 2HDM WITH A HIGGS-PHOBIK PSEUDOSCALAR BOSON

The 2HDM introduces two  $SU(2)_L$  complex scalar doublet fields with hypercharge  $Y = +1$ ,  $\Phi_1$  and  $\Phi_2$  [113]:

$$\Phi_i = \begin{pmatrix} w_i^+ \\ \frac{v_i + \rho_i + i\eta_i}{\sqrt{2}} \end{pmatrix}, \quad (i = 1, 2) \quad (3)$$

where  $v_1$  and  $v_2$  are the vacuum expectation values of  $\Phi_1$  and  $\Phi_2$ , respectively. The ratio of  $v_2$  to  $v_1$  defines  $\tan\beta \equiv v_2/v_1$ .<sup>1</sup> The electroweak symmetry is broken by  $v = \sqrt{v_1^2 + v_2^2} = 246$  GeV. We introduce a discrete  $Z_2$  symmetry to prevent the tree-level flavor-changing neutral currents (FCNC) [114,115], under which  $\Phi_1 \rightarrow \Phi_1$  and  $\Phi_2 \rightarrow -\Phi_2$ . Allowing the softly broken  $Z_2$  symmetry and retaining the  $CP$  invariance, we write the scalar potential as

$$\begin{aligned} V_\Phi = & m_{11}^2 \Phi_1^\dagger \Phi_1 + m_{22}^2 \Phi_2^\dagger \Phi_2 - m_{12}^2 (\Phi_1^\dagger \Phi_2 + \text{H.c.}) \\ & + \frac{1}{2} \lambda_1 (\Phi_1^\dagger \Phi_1)^2 + \frac{1}{2} \lambda_2 (\Phi_2^\dagger \Phi_2)^2 + \lambda_3 (\Phi_1^\dagger \Phi_1) (\Phi_2^\dagger \Phi_2) \\ & + \lambda_4 (\Phi_1^\dagger \Phi_2) (\Phi_2^\dagger \Phi_1) + \frac{1}{2} \lambda_5 [(\Phi_1^\dagger \Phi_2)^2 + \text{H.c.}] \end{aligned} \quad (4)$$

The 2HDM accommodates five physical Higgs bosons, the lighter  $CP$ -even scalar  $h$ , the heavier  $CP$ -even scalar  $H$ , the  $CP$ -odd pseudoscalar  $A$ , and a pair of charged Higgs bosons  $H^\pm$ . For the relations of the mass eigenstates with the weak eigenstates via two mixing angles of  $\alpha$  and  $\beta$ , we refer the reader to Ref. [116]. The SM Higgs boson  $h_{\text{SM}}$  is a linear combination of  $h$  and  $H$ , given by

$$h_{\text{SM}} = s_{\beta-\alpha} h + c_{\beta-\alpha} H. \quad (5)$$

Two scenarios exist in explaining the SM-like Higgs boson [117–119], the normal scenario where  $h$  is observed and the inverted scenario where  $H$  is observed while  $h$  has been hidden [54,103,120]. This work focuses on the normal scenario, i.e.,  $m_h = 125$  GeV. Then, the Higgs coupling modifier for a gauge boson pair,  $W^+W^-$  and  $ZZ$ , becomes

$$\kappa_V = s_{\beta-\alpha}. \quad (6)$$

If  $|s_{\beta-\alpha}| = 1$ , the couplings of  $h$  to the SM particles are the same as in the SM, which is called the Higgs alignment.

The quartic couplings in Eq. (4) play a crucial role in governing the perturbativity, unitarity, and vacuum

<sup>1</sup>In what follows, we will use the simplified notation of  $s_x = \sin x$ ,  $c_x = \cos x$ , and  $t_x = \tan x$ .

stability. Near the Higgs alignment limit, the quartic couplings are [121]

$$\begin{aligned}\lambda_1 &\simeq \frac{1}{v^2} [m_h^2 + t_\beta^2 (M_H^2 - M^2)], \\ \lambda_2 &\simeq \frac{1}{v^2} \left[ m_h^2 + \frac{1}{t_\beta^2} (M_H^2 - M^2) \right], \\ \lambda_3 &\simeq \frac{1}{v^2} [m_h^2 - M_H^2 - M^2 + 2M_{H^\pm}^2], \\ \lambda_4 &\simeq \frac{1}{v^2} [M^2 + M_A^2 - 2M_{H^\pm}^2], \\ \lambda_5 &\simeq \frac{1}{v^2} [M^2 - M_A^2],\end{aligned}\quad (7)$$

where  $M^2 = m_{12}^2/(s_\beta c_\beta)$ . When  $t_\beta$  is large, the perturbativity of  $\lambda_1$  is particularly important [103]. The  $t_\beta^2$  terms in  $\lambda_1$  easily break the perturbativity and unitarity unless  $M^2$  is almost the same as  $M_H^2$ . The perturbativities of  $\lambda_4$  and  $\lambda_5$  with  $M^2 \approx M_H^2$  demand  $M_H$  similar to  $M_A$  and  $M_{H^\pm}$ :

$$M \approx M_H \sim M_A \sim M_{H^\pm}, \quad (8)$$

where  $M = \sqrt{M^2}$ .

The Yukawa interactions of the SM fermions are parametrized by

$$\begin{aligned}\mathcal{L}_{\text{Yuk}} &= -\sum_f \left( \frac{m_f}{v} \xi_f^h \bar{f} f h + \frac{m_f}{v} \xi_f^H \bar{f} f H - i \frac{m_f}{v} \xi_f^A \bar{f} \gamma_5 f A \right) \\ &\quad - \left\{ \frac{\sqrt{2}}{v} \bar{t} (m_t \xi_t^A P_- + m_b \xi_b^A P_+) b H^+ \right. \\ &\quad \left. + \sum_{\ell=\mu,\tau} \frac{\sqrt{2} m_\ell}{v} \xi_\ell^A \bar{\nu}_\ell P_+ \ell H^+ + \text{H.c.} \right\},\end{aligned}\quad (9)$$

where  $P_\pm = (1 \pm \gamma^5)/2$ . The Higgs coupling modifiers in type-X are

$$\begin{aligned}\xi_{t,b}^h &= s_{\beta-\alpha} + \frac{c_{\beta-\alpha}}{t_\beta}, & \xi_\ell^h &= s_{\beta-\alpha} - c_{\beta-\alpha} t_\beta, \\ \xi_{t,b}^H &= \frac{s_\alpha}{s_\beta}, & \xi_\ell^H &= \frac{c_\alpha}{c_\beta}, & \xi_\ell^A &= \frac{1}{\xi_t^A} = -\frac{1}{\xi_b^A} = t_\beta.\end{aligned}\quad (10)$$

For the trilinear scalar couplings, we parametrize the Lagrangian as

$$\begin{aligned}\mathcal{L}_{\text{tri}} &= v \left[ \frac{1}{3!} \sum_{\varphi_0} \hat{\lambda}_{\varphi_0^3} \varphi_0^3 + \frac{1}{2} \hat{\lambda}_{hhH} hhH + \frac{1}{2} \hat{\lambda}_{hHH} hHH \right. \\ &\quad \left. + \sum_{\varphi_0} \left\{ \frac{1}{2} \hat{\lambda}_{\varphi_0 AA} A^2 \varphi_0 + \lambda_{\varphi_0 H^+ H^-} H^+ H^- \varphi_0 \right\} \right],\end{aligned}\quad (11)$$

where  $\varphi_0 = h, H$ .

Our central concern is the exotic decay of the observed Higgs boson,  $h \rightarrow AA$ , which is severely restricted by the current Higgs precision data [117–119]. Since the muon  $g-2$  anomaly requires a light pseudoscalar boson and  $h \rightarrow AA^* \rightarrow A\tau^+\tau^-$  also constrains the model for  $M_A > m_h/2$ , we need to forbid the  $h$ - $A$ - $A$  vertex. So we consider type-X with the Higgs-phobic pseudoscalar boson  $A$ , simply called the Higgs-phobic type-X in what follows. The trilinear coupling for the vertex is

$$\begin{aligned}\hat{\lambda}_{hAA} &= \frac{1}{4s_\beta c_\beta} [(2M_A^2 - m_h^2)c_{\alpha-3\beta} \\ &\quad - (2M_A^2 + 3m_h^2 - 4M^2)c_{\alpha+\beta}].\end{aligned}\quad (12)$$

Since  $s_{\beta-\alpha}$  and  $c_{\beta-\alpha}$  are useful when dealing with the Higgs precision data, we use the identities of

$$\begin{aligned}\frac{c_{\alpha-3\beta}}{s_\beta c_\beta} &= -2s_{\beta-\alpha} - \left( t_\beta - \frac{1}{t_\beta} \right) c_{\beta-\alpha}, \\ \frac{c_{\alpha+\beta}}{s_\beta c_\beta} &= 2s_{\beta-\alpha} - \left( t_\beta - \frac{1}{t_\beta} \right) c_{\beta-\alpha},\end{aligned}\quad (13)$$

and rewrite  $\hat{\lambda}_{hAA}$  as

$$\hat{\lambda}_{hAA} = (2M^2 - 2M_A^2 - m_h^2)s_{\beta-\alpha} + (m_h^2 - M^2) \left( t_\beta - \frac{1}{t_\beta} \right) c_{\beta-\alpha}.\quad (14)$$

Then, the condition of  $\hat{\lambda}_{hAA} = 0$  accords with

$$\text{Higgs-phobic } A: \frac{s_{\beta-\alpha}}{c_{\beta-\alpha}} = - \left( t_\beta - \frac{1}{t_\beta} \right) \frac{m_h^2 - M^2}{2M^2 - 2M_A^2 - m_h^2}.\quad (15)$$

Note that the exact Higgs alignment cannot coexist with the Higgs-phobic  $A$ . Since  $s_{\beta-\alpha}$  is determined by  $t_\beta$ ,  $M^2$ , and  $M_A$ , the model has five parameters of

$$\{t_\beta, M_A, M_H, M_{H^\pm}, M^2\}.\quad (16)$$

An interesting consequence of the Higgs-phobic  $A$  is that the Higgs alignment naturally arises, although not exact. In Fig. 1, we show  $s_{\beta-\alpha}$  as a function of  $M$  satisfying Eq. (15). Here we take the positive  $c_{\beta-\alpha}$  scheme as in the public codes of 2HDMC [122], HIGGSIGNALS [123], and HIGGSBOUNDS [124]. In Fig. 1, two cases are considered,  $M_A = 70$  GeV (left panel) and  $M_A = 300$  GeV (right panel), with  $t_\beta = 100$ . In both cases,  $|s_{\beta-\alpha}| \approx 1$  in the most range of  $M$ . If we restrict ourselves to  $M \sim M_A$ , as shown by the colored regions corresponding to  $M \in [0.5M_A, 2M_A]$ , the preference for the alignment is greater.

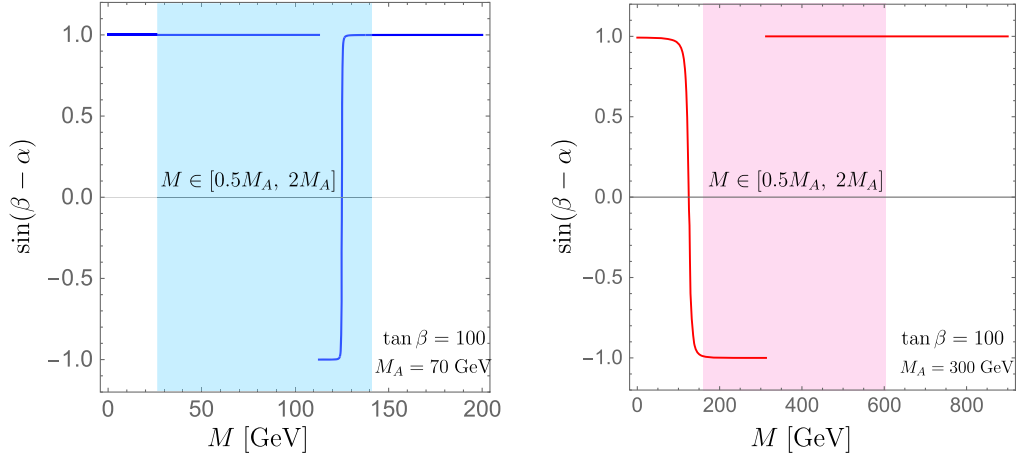


FIG. 1.  $\sin(\beta - \alpha)$  as a function of  $M (\equiv \sqrt{M^2})$  in the Higgs-phobic type-X. For  $t_\beta = 100$ , we consider  $M_A = 70$  GeV (left) and  $M_A = 300$  GeV (right). The colored regions correspond to  $M \in [0.5M_A, 2M_A]$ .

Brief comments on the wrong-sign Yukawa coupling of the tau lepton are in order here. The current Higgs precision data still allow the possibility that  $\kappa_V$  and  $\xi_{b,\tau}^h$  have opposite signs. In the literature, the LHC phenomenology of the wrong-sign  $b$  quark Yukawa coupling in type-II has been extensively studied [125–129]. In type-X with large  $t_\beta$ , however,  $\xi_b^h$  has the same sign with  $\kappa_V$ . Wrong-sign Yukawa coupling is only possible for the tau lepton. In the positive  $c_{\beta-\alpha}$  scheme, caution is needed since the negative sign of  $\xi_\tau^h$  does not mean the wrong-sign  $\tau$  Yukawa coupling. If  $s_{\beta-\alpha} = -1$ , all of the Higgs coupling modifiers have negative sign as  $\kappa_V = \xi_{t,b,\tau}^h = -1$ , which indicates the right-sign. In summary, the right-sign and wrong-sign of the tau lepton Yukawa coupling are defined by

$$\begin{aligned} \text{right-sign: } & \xi_\tau^h \times \text{sgn}(s_{\beta-\alpha}) > 0; \\ \text{wrong-sign: } & \xi_\tau^h \times \text{sgn}(s_{\beta-\alpha}) < 0. \end{aligned} \quad (17)$$

### III. SCANNING STRATEGIES AND THE RESULTS

Focusing on the Higgs-phobic type-X, we study the implication of the CDF  $m_W$  and muon  $g - 2$  anomalies as well as the other theoretical and experimental constraints. Over the randomly generated parameters in the ranges of

$$\begin{aligned} t_\beta & \in [1, 200], \quad m_{12}^2 \in [0, 15000] \text{ GeV}^2, \\ M_H & \in [130, 1000] \text{ GeV}, \quad M_A \in [10, 200] \text{ GeV}, \\ M_{H^\pm} & \in [80, 1000] \text{ GeV}, \end{aligned} \quad (18)$$

we cumulatively enforce the following constraints in four steps<sup>2</sup>:

<sup>2</sup>An important constraint is from flavor physics like  $b \rightarrow s\gamma$  [135,136]. In type-X, the region with small  $t_\beta$  and the light charged Higgs boson is significantly constrained:  $\tan\beta > 2.7(2.6)$  for  $M_{H^\pm} = 110(140)$  GeV [135]. But the observed  $\Delta a_\mu$  requires large  $t_\beta$ , for which the FCNC processes do not affect.

- (1) *step I:  $\Delta a_\mu + \text{theory}$* 
  - (a) First, we obtain  $s_{\beta-\alpha}$  from the model parameters in Eq. (16) parameters by using the Higgs-phobic condition in Eq. (15). For efficient scanning, we preliminary demand  $0.8 < |s_{\beta-\alpha}| < 1$ , considering the most updated results on the Higgs coupling modifiers [117].
  - (b) We demand the bounded-from-below potential [137], the unitarity of scalar-scalar scatterings [113,138], the perturbativity of Higgs quartic couplings [120], and the stability of the vacuum [139–141].
  - (c) We require that the model explains  $\Delta a_\mu$  in Eq. (2). The contributions to  $\Delta a_\mu$  in the 2HDM are summarized in Appendix A.

- (2) *step II: EWPD + step I*

We consider the Peskin-Takeuchi oblique parameters  $S$  and  $T$  with  $U = 0$  before and after the CDF  $m_W$  measurement [4], called the PDG and CDF cases, respectively:

$$\begin{aligned} \text{PDG: } S_{\text{PDG}} & = 0.05 \pm 0.08, & T_{\text{PDG}} & = 0.09 \pm 0.07, \\ \rho_{\text{PDG}} & = 0.92, \end{aligned} \quad (19)$$

$$\begin{aligned} \text{CDF: } S_{\text{CDF}} & = 0.15 \pm 0.08, & T_{\text{CDF}} & = 0.27 \pm 0.06, \\ \rho_{\text{CDF}} & = 0.93, \end{aligned} \quad (20)$$

where  $\rho$  is the correlation between  $S$  and  $T$ . In the 2HDM, the oblique parameters have been extensively studied [142–149]. We use the public code 2HDMC [122], which adopt the calculation of Refs. [147,148]. Then, we perform the  $\chi^2$  analysis in the  $(S, T)$  plane, requiring  $p > 0.05$ .

- (3) *step III: Collider + step II*

- (a) The Higgs precision data are checked via the public code HIGGSIGNALS-v2.6.2 [123] which

takes into account 111 Higgs observables [150–157]. Since our model has five parameters, the number of degrees of freedom is 106. Based on the  $\chi^2$  value from the HIGGSIGNALS, we demand that the  $p$ -value should be larger than 0.05.

- (b) The direct searches for BSM Higgs bosons at the LEP, Tevatron, and LHC are examined by using the open code HIGGSBOUNDS-v5.10.2 [124]. We exclude a parameter point if any cross section predicted by the model exceeds the observed 95% C.L. upper bound.

(4) *step IV: LFU + step III*

We perform a global  $\chi^2$  fit of the Higgs-phobic type-X to  $\Delta a_\mu$  and the following LFU data:

- (a) For the  $\tau$  decay, we adopt the HFLAV global fit results of [158]

$$\frac{g_\tau}{g_\mu}, \frac{g_\tau}{g_e}, \frac{g_\mu}{g_e}, \left(\frac{g_\tau}{g_\mu}\right)_\pi, \left(\frac{g_\tau}{g_\mu}\right)_K. \quad (21)$$

One redundant degree of freedom should be removed since it has a zero eigenvalue in the covariance matrix.

- (b) We include the Michel parameters [159,160] from the energy and angular distributions of  $\ell^-$  in the decay of  $\tau^- \rightarrow \ell^- \nu \nu_\tau$ :

$$\rho_e, (\xi\delta)_e, \xi_e, \eta_\mu, \rho_\mu, (\xi\delta)_\mu, \xi_\mu, \xi_\pi, \xi_\rho, \xi_{a_1}. \quad (22)$$

- (c) We also include the accurate measurement of the leptonic  $Z$  decays. Two ratios of the partial decay rates are considered [161]:

$$\frac{\Gamma(Z \rightarrow \mu^+ \mu^-)}{\Gamma(Z \rightarrow e^+ e^-)}, \quad \frac{\Gamma(Z \rightarrow \tau^+ \tau^-)}{\Gamma(Z \rightarrow e^+ e^-)}. \quad (23)$$

The theoretical calculations of the LFU observable in type-X are summarized in Appendix B and the experimental data are referred to Ref. [103]. Including  $\Delta a_\mu$ , we have 17 independent observables in the global fit. Since the model parameters have already been restricted through step I, II, and III, we consider the number of degrees of freedom to be  $N_{\text{dof}} = 17$  and demand the  $p$ -value larger than 0.01. In the SM, the  $p$ -value is only 0.003 [103].

We randomly scan the five-dimensional parameter space in Eq. (18). For the PDG and CDF cases, we independently obtained  $10^7$  parameter points that pass step I. Setting step I as the reference, we calculate the survival probabilities at each step:

$$\begin{aligned} \text{PDG: } P_{\text{step II}} &= 5.47\%, & P_{\text{step III}} &= 3.15\%, \\ & P_{\text{step IV}} &= 0.62\%, \\ \text{CDF: } P_{\text{step II}} &= 1.56\%, & P_{\text{step III}} &= 1.00\%, \\ & P_{\text{step IV}} &= 0.21\%. \end{aligned} \quad (24)$$

The Higgs-phobic type-X does have considerable parameter points that explain all the constraints. The validity of the model is largely irrelevant to whether we take the PDG or CDF case, but the survival probabilities are different. The PDG case has approximately three times greater probability than the CDF. But just because the PDG case has more viable parameter points does not mean it is a better solution.

Now we investigate which constraint excludes which region of the parameter space. First, we present  $t_\beta$  versus  $M_A$  at step I in Fig. 2, which is common for the PDG and CDF cases. The color code indicates  $\Delta a_\mu$ . The observed  $\Delta a_\mu$  allows the band shape in  $(M_A, t_\beta)$ . We need large  $t_\beta$  above  $\sim 35$  and light  $M_A$  below  $\sim 170$  GeV.  $M_A$  above 170 GeV is also feasible if  $t_\beta$  is greater than 200. But we avoid too large  $t_\beta$  to retain the perturbativity of the Yukawa coupling of the tau lepton to the BSM Higgs bosons.

As we go through the remaining steps, the masses of the other BSM Higgs bosons are also constrained. In Fig. 3, we show  $M_{H^\pm}$  versus  $M_A$  with the color code of  $M_H$  at step II (left panels), step III (middle panels), and step IV (right panels). We compare the PDG case (upper panels) with the CDF (lower panels). Let us begin with their common features. The first and most important one is that upper bounds exist on the masses of new Higgs bosons, which appear in step II. It is because the light  $M_A$ , which is

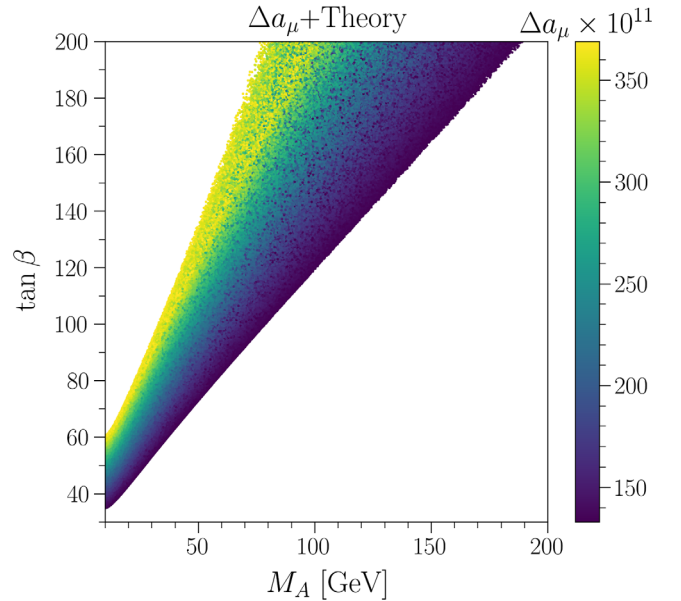


FIG. 2. Allowed regions of  $(M_A, \tan \beta)$  at step I with  $\Delta a_\mu$  and the theoretical constraints. The color code indicates  $\Delta a_\mu$ .

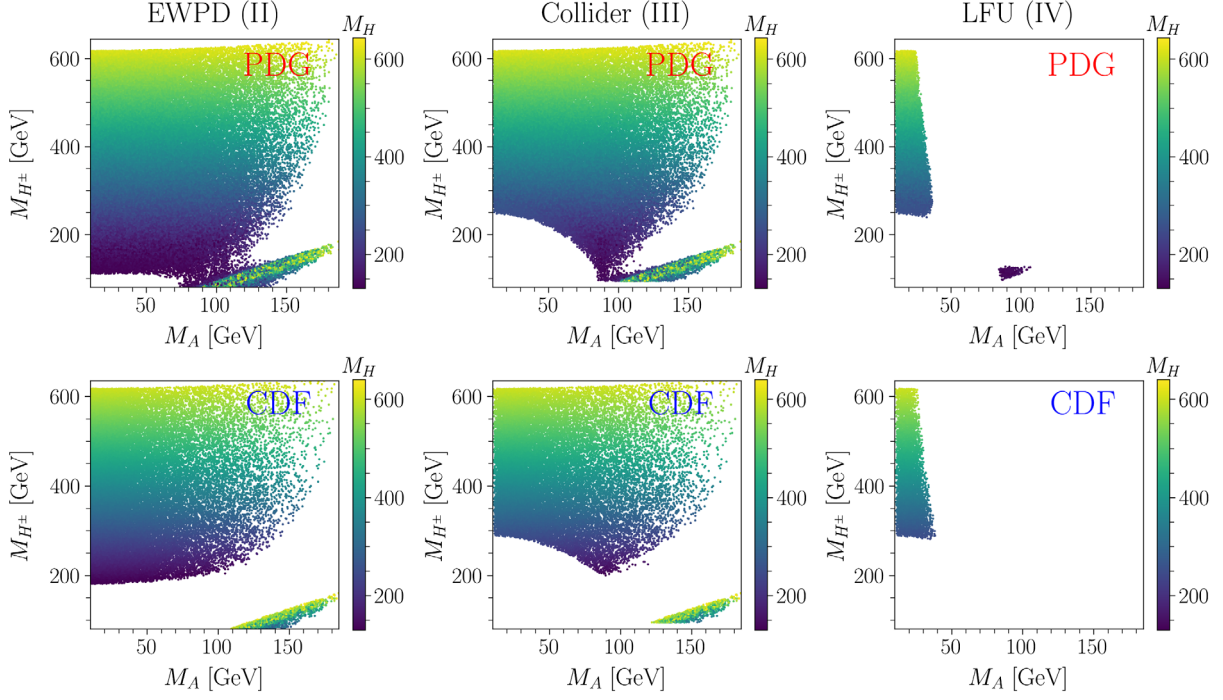


FIG. 3.  $M_{H^\pm}$  versus  $M_A$  at step II (left), step III (middle), and step IV (right), with the color code indicating  $M_H$ . We consider the PDG case (upper) and the CDF case (lower).

required to explain  $\Delta a_\mu$ , brings down  $M_H$  and  $M_{H^\pm}$  to yield small  $S$  and  $T$ . The upper bounds on  $M_H$  and  $M_{H^\pm}$  remain almost intact to the last step such that  $M_{H,H^\pm} \lesssim 600$  GeV in both cases.

The second common feature is the exclusion of the lower-left corner in  $(M_A, M_{H^\pm})$  at step III (Collider), mainly from  $h \rightarrow \tau^+ \tau^-$ . In Fig. 4, we show for the CDF case  $M_{H^\pm}$  versus  $M_A$  with the color code of  $|\xi_\tau^h|$  (left panel) and  $c_{\beta-\alpha}$  (right panel) over the parameter points that pass step II (EWPD). As can be seen in the left panel of Fig. 4,

the area that disappears as we go from step II to step III in Fig. 3 almost coincides with the region of too large  $|\xi_\tau^h|$ . This behavior is attributed to  $\xi_\tau^h$  in Eq. (10). When the Higgs alignment is broken even a little, large  $t_\beta$  increases  $|\xi_\tau^h|$  unacceptably. To reveal the feature in more detail, we present  $c_{\beta-\alpha}$  via the color code over the plane of  $(M_A, M_{H^\pm})$  in the right panel of Fig. 4. The region with light  $M_A$  and light  $M_{H^\pm}$  has relatively sizable  $c_{\beta-\alpha}$ , which further enhances  $|\xi_\tau^h|$ . So, the exclusion by  $h \rightarrow \tau^+ \tau^-$  results in the lower bound on  $M_{H^\pm}$  for light  $M_A$ .

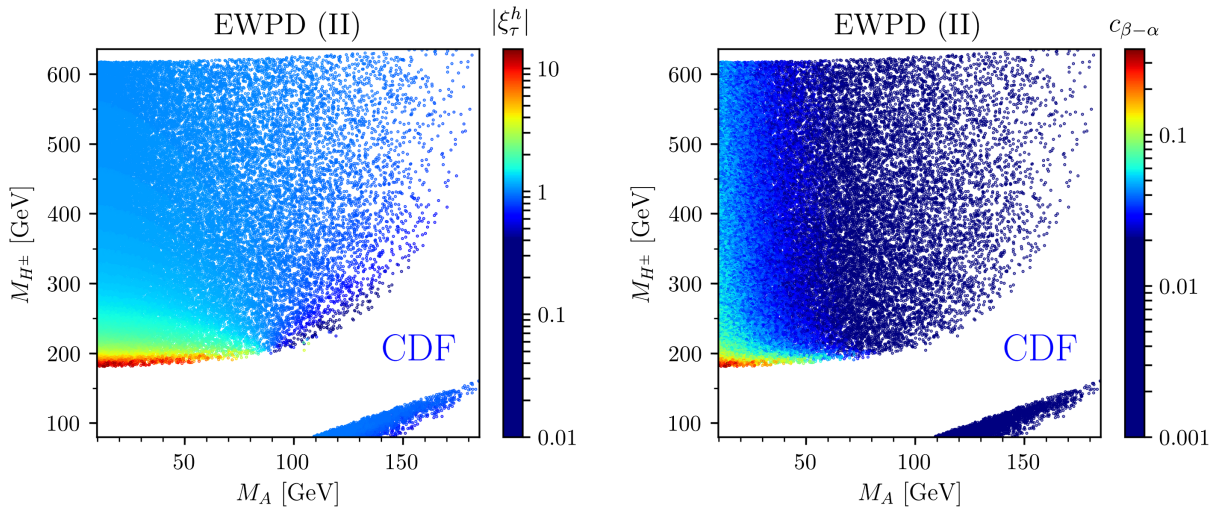


FIG. 4. For the parameter points that pass step II,  $M_{H^\pm}$  versus  $M_A$  with the color code of  $|\xi_\tau^h|$  (left) and with the color code of  $c_{\beta-\alpha}$  (right). We focus on the CDF case.

The third common feature is that the global fit to  $\Delta a_\mu$  and the LFU data removes most of the parameter space with  $M_A \gtrsim 38$  GeV: the exceptional island-shaped region in the PDG case is deferred until we discuss the differences between the PDG and CDF cases. The exclusion of  $M_A \gtrsim 38$  GeV is primarily from the tree-level contributions to the lepton flavor violating decays of the tau lepton, mediated by the charged Higgs boson. The key parameter is [103]

$$\delta_{\text{tree}} = \frac{m_\mu m_\tau t_\beta^2}{M_{H^\pm}^2}. \quad (25)$$

Large  $t_\beta$ , which corresponds to heavy  $M_A$  because of  $\Delta a_\mu$ , blows up the  $\chi_{\text{LFU}}^2$  value. So only the region with very light  $M_A$  is finally allowed.

Even though the PDG and CDF cases share many common features, significant differences also exist. The first noticeable difference is the island-shaped region at step IV in the PDG case. To facilitate discussion below, let us call this special region the PDG-island and call the bulk region with  $M_A \lesssim 38$  GeV the mainland. The parameters in the PDG-island are populated around

$$\begin{aligned} \text{PDG-island: } M_H &\in [130.0, 165.3] \text{ GeV,} \\ M_A &\in [84.1, 111.9] \text{ GeV,} \\ M_{H^\pm} &\in [96.5, 127.9] \text{ GeV,} \quad t_\beta > 154.9. \end{aligned} \quad (26)$$

In the CDF case, however, the parameter points in Eq. (26) are excluded from step II. To understand the origin, let us present the oblique parameter  $T$  in the limit of  $M_A \simeq M_H \simeq M_{H^\pm}$ :

$$T \simeq \frac{\Delta M_A \Delta M_H}{12\pi^2 \alpha v^2}, \quad \text{if } M_{H^\pm} \simeq M_A \simeq M_H, \quad (27)$$

where  $\Delta M_i = M_i - M_{H^\pm}$ . The  $T_{\text{CDF}}$  in Eq. (20) requires  $\Delta M_{A,H} \gtrsim 80$  GeV that the PDG-island cannot satisfy. On the contrary,  $T_{\text{PDG}}$  permits the mass degeneracy among BSM Higgs bosons, which the PDG-island requires.

An important question about the PDG-island is how it can evade the most profound constraints from the LFU data. As discussed before, the key parameter  $\delta_{\text{tree}}$  in Eq. (25) requires small  $t_\beta$  and thus light  $M_A$ . But there exists an alternative way to evade the LFU constraints through another key parameter of

$$e_{\tau}^{\tau} = \delta_{\text{tree}} \left[ \frac{\delta_{\text{tree}}}{8} - \frac{m_\mu g(\rho_\tau^\mu)}{m_\tau f(\rho_\tau^\mu)} \right], \quad (28)$$

where  $g(x)$ ,  $f(x)$ , and  $\rho_j^i$  are referred to Appendix B. If the first and second terms in Eq. (28) are exquisitely canceled, the value of  $\chi_{\text{LFU}}^2$  can be substantially reduced. The cancellation demands a relation of  $M_{H^\pm}$  to  $t_\beta$ . In Fig. 5, we show  $M_{H^\pm}$  versus  $t_\beta$  with the color code of  $\chi_{\text{LFU}}^2$  over the

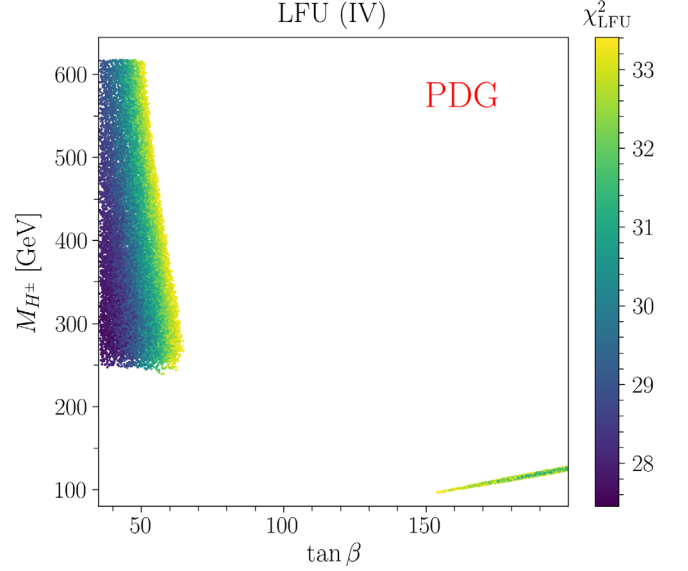


FIG. 5.  $M_{H^\pm}$  versus  $t_\beta$  at step IV with the color code indicating  $\chi_{\text{LFU}}^2$ . We focus on the PDG case.

finally allowed parameter points in the PDG case. Here we only show the parameter points with  $\chi_{\text{LFU}}^2 < 33.41$ , i.e.,  $p > 0.01$  with 17 degrees of freedom. It is clearly seen that the minimum of  $\chi_{\text{LFU}}^2$  occurs in the mainland region with  $M_{H^\pm} \gtrsim 250$  GeV and  $t_\beta \simeq 35$ . Almost all the parameter points outside the mainland have  $p$ -value below 0.01. Exceptional is the band-shape PDG-island with  $M_{H^\pm} \in [96.5, 127.9]$  GeV and  $t_\beta > 154.9$ , which accommodates the cancellation in Eq. (28).

The second difference between the PDG and CDF cases is the lower bound on  $M_{H^\pm}$  for  $M_A \lesssim 38$  GeV:  $M_{H^\pm} \gtrsim 250$  GeV in the PDG case while  $M_{H^\pm} \gtrsim 300$  GeV in the CDF case. The difference begins in step II. When  $M_A \ll M_{H^\pm}$ ,  $S$  and  $T$  are approximated into

$$\begin{aligned} S &\simeq -\frac{5}{72\pi}, \\ T &\simeq -\frac{M_{H^\pm} \Delta M_H}{16\pi^2 \alpha v^2} \left[ 1 - \frac{\Delta M_H}{6M_{H^\pm}} + \mathcal{O}\left(\frac{\Delta M_H^3}{M_{H^\pm}^3}\right) \right]. \end{aligned} \quad (29)$$

The positive  $T_{\text{CDF}}$  in Eq. (20) prefers negative and nonzero  $\Delta M_H$  for light  $M_A$ . Therefore, the heavy mass of  $H$ , above 125 GeV by definition, pushes up the lower bound on  $M_{H^\pm}$  in the CDF case. The substantial mass gap between  $M_A$  and  $M_{H^\pm}$  guarantees the dominant decay mode of  $H^\pm \rightarrow W^\pm A$ . In the PDG case, there are two different regions in the charged Higgs boson phenomenology, the mainland region with  $M_{H^\pm} \gtrsim 250$  GeV and the island region with  $M_{H^\pm} \simeq 100$  GeV.

The third difference is found in the allowed  $t_\beta$  and  $s_{\beta-\alpha}$ . In Fig. 6, we present  $t_\beta$  versus  $|s_{\beta-\alpha}|$  with the color code of  $M_{H^\pm}$  at step II (left), step III (middle), and step IV (right). We compare the results of the PDG (upper) with those of

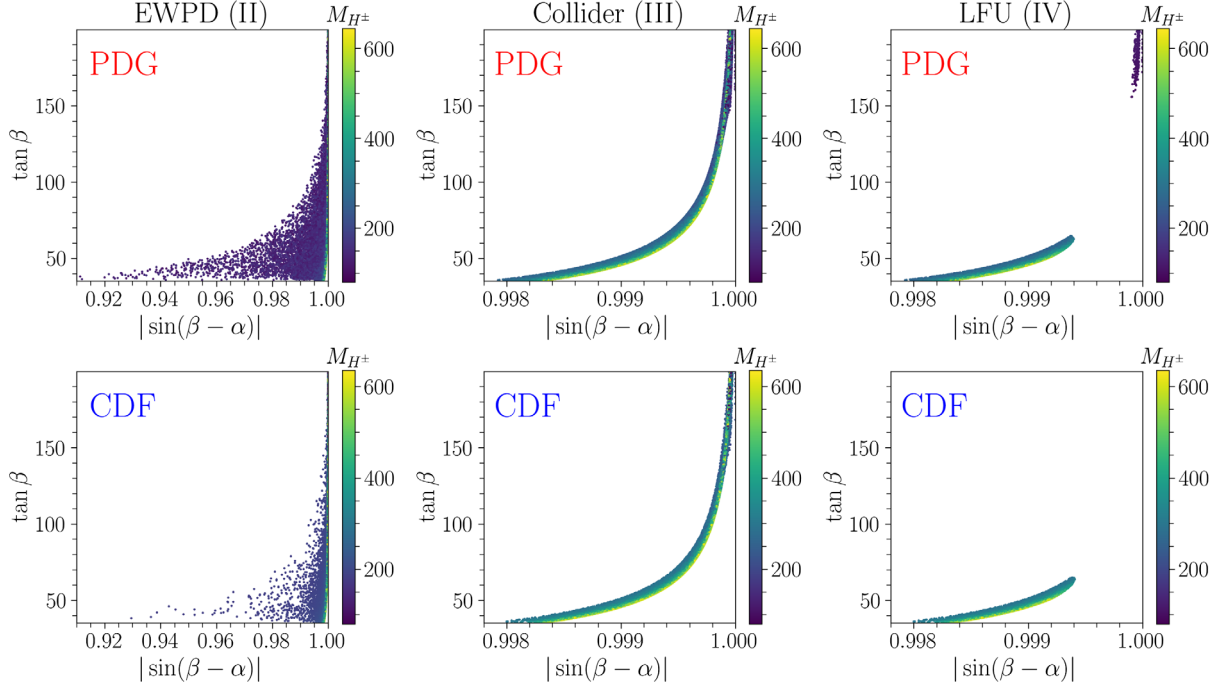


FIG. 6.  $\tan\beta$  versus  $|\sin(\beta - \alpha)|$  with color code of  $M_{H^\pm}$  at step II (left), step III (middle), and step IV (right). We compare the PDG (upper) and the CDF (lower).

the CDF (lower). The generic feature of the Higgs-phobic type-X, the almost exact Higgs alignment, appears from step II. When imposing the Higgs precision data at step III, the tendency toward the Higgs alignment is stronger. A dramatic change occurs in step IV. Large  $t_\beta$  above  $\sim 65$  is excluded in the CDF case. In the PDG case, however, the region with  $t_\beta \in [170, 200]$  and  $|s_{\beta-\alpha}| \approx 1$  remains, corresponding to the PDG-island.

The last difference is the sign of the tau lepton Yukawa coupling. Considering the definitions of the right-sign and wrong-sign  $\tau$  Yukawa coupling in Eq. (17), we present  $\xi_\tau^h \times \text{sgn}(s_{\beta-\alpha})$  via color codes over the parameter space of  $(M_A, M_{H^\pm})$  in Fig. 7. The mainland with  $M_A \lesssim 38$  GeV, in the PDG and CDF cases, has wrong-sign  $\tau$  Yukawa coupling, as discussed in Ref. [112]. In the PDG-island, however, right-sign  $\tau$  Yukawa coupling is also possible in a sizable portion, about 10%, of the finally allowed parameter space. It is attributed to almost 100% alignment in the PDG-island (see Fig. 7): if  $c_{\beta-\alpha}$  is small enough to suppress the large  $t_\beta$  in Eq. (10),  $\xi_\tau^h$  and  $s_{\beta-\alpha}$  have the same sign. Probing the wrong-sign  $\tau$  Yukawa coupling at the LHC will give us an important implication on the PDG-island.

#### IV. CUTOFF SCALES VIA THE RGE ANALYSIS

Now that the Higgs-phobic type-X is shown to explain all the constraints, a question arises as to what energy scale this model is valid. To answer the question, we run each parameter point via the RGE and check three conditions—unitarity, perturbativity, and vacuum stability—

increasing the energy scale. If any condition is broken at a particular energy scale, we stop the evolution and record the energy scale as the cutoff scale  $\Lambda_c$ .

We use the public code 2HDME [162,163] to run the following parameters:

$$g_s, g, g', \lambda_{1,\dots,5}, \xi_f^{h,HA}, m_{ij}^2, v_i, (i=1,2). \quad (30)$$

First, we convert the model parameters in Eq. (16) and Eq. (30). The top quark pole mass of  $m_t^{\text{pole}} = 173.4$  GeV is used to match the 2HDM to the SM parameters. The

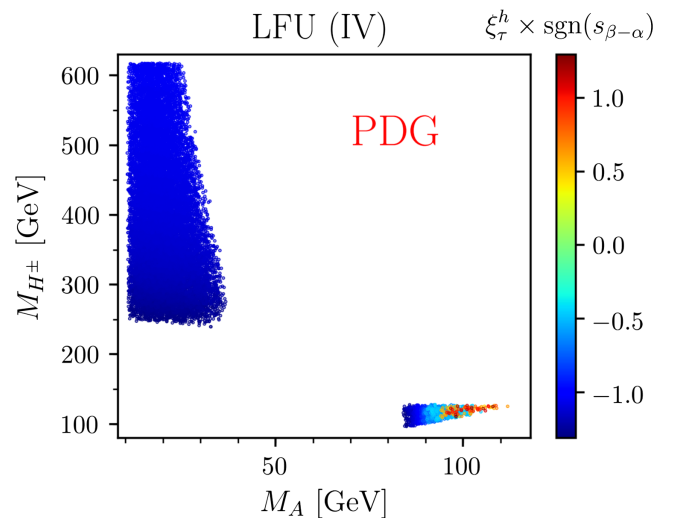


FIG. 7.  $M_{H^\pm}$  versus  $M_A$  with the color code of  $\xi_\tau^h \times \text{sgn}(s_{\beta-\alpha})$  in the PDG case.



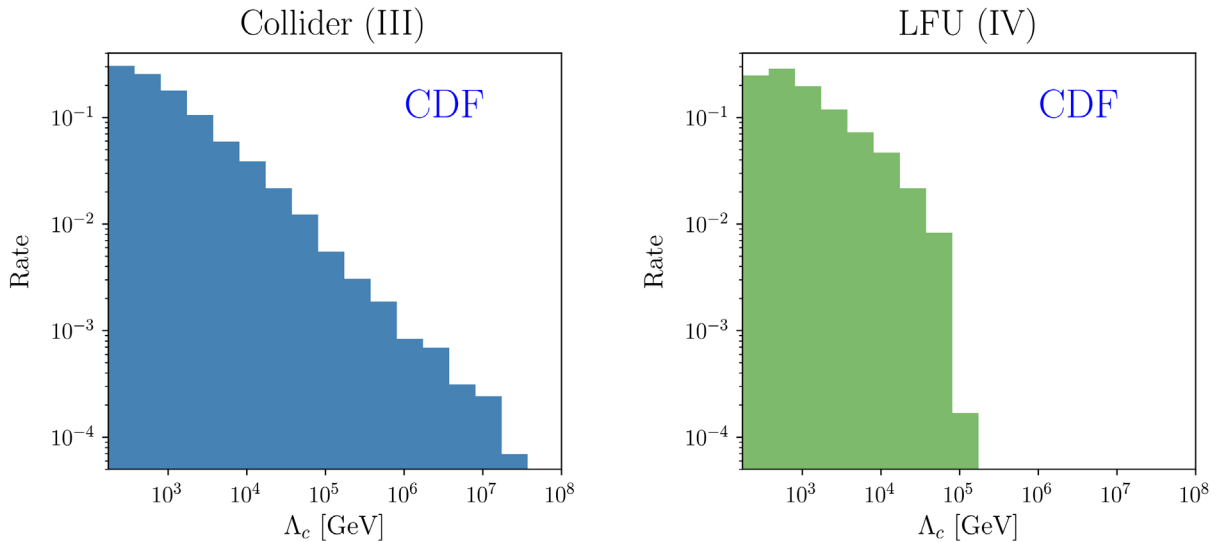


FIG. 8. Distributions of the cutoff scales of the parameter points at step III (left) and step IV (right) in the CDF case.

boundary conditions at  $m_t^{\text{pole}}$  are referred to Ref. [162]. And we evolve them into higher energy scale through the one-loop RGE.<sup>3</sup>

To present the high energy scale behavior of all the viable parameter points, we show the distribution of  $\Lambda_c$  in Fig. 8, focusing on the CDF case. We compare the  $\Lambda_c$  distribution of the parameter points at step III (left panel) with those at step IV (right panel). The “rate” in the y-axis denotes the ratio  $N_{\Lambda_c}/N_{\text{step}}$ , where  $N_{\Lambda_c}$  is the number of the parameter points with the cutoff scale  $\Lambda_c$  and  $N_{\text{step}}$  is the total number of the parameter points at step III (left panel) and at step IV (right panel). At step III, the Higgs-phobic type-X is stable up to about  $10^7$  GeV. After step IV, however, the model is valid only up to about  $10^5$  GeV. Although the Higgs-phobic type-X is a viable model at the electroweak scale, it needs an extension at the energy scale not far from the LHC reach. Future colliders at  $\sqrt{s} = 100$  TeV, such as the Future hadron-hadron Circular Collider (FCC-hh) at CERN [164] and the CEPC [165,166], are expected to find a hint of the next-level BSM model.

If we further require a high cutoff scale, the parameter space is considerably constrained. For  $\Lambda_c > 1$  TeV, the surviving probability is almost halved. If  $\Lambda_c > 10$  TeV, the survival probability in the CDF case goes down to 0.01% with the parameter points of

$$\begin{aligned}
 \text{if } \Lambda_c^{\text{CDF}} > 10 \text{ TeV: } & M_A \in [11, 38] \text{ GeV,} \\
 & M_H \in [249, 306] \text{ GeV, } M_{H^\pm} \in [283, 338] \text{ GeV,} \\
 & M \in [249, 306] \text{ GeV,} \\
 & t_\beta \in [36.6, 64.7].
 \end{aligned} \tag{31}$$

<sup>3</sup>The two-loop results are not substantially different from the one-loop results.

Since the BSM Higgs boson masses are within the LHC reach, we expect that the HL-LHC can probe the model with high  $\Lambda_c$ .

The final discussion is on the difference in the high-energy scale behaviors between the PDG and CDF cases. In Fig. 9, we present the cutoff scales via the color code in the finally allowed  $(M_A, M_{H^\pm})$ . The left (right) panel shows the results in the PDG (CDF) case. The difference is clear. The PDG case can accommodate a larger cutoff scale. In the mainland region with  $M_A \lesssim 38$  GeV,  $\Lambda_c$  can go up to  $10^6$  GeV, which is about ten times higher than  $\Lambda_c$  in the CDF case. In the PDG-island, the cutoff scale is much higher up to about  $10^7$  GeV. In terms of the high energy scale stability, the PDG-island is the most attractive.

## V. GOLDEN DISCOVERY CHANNELS AT THE LHC

For the LHC phenomenology of the Higgs-phobic type-X, we first study the branching ratios of the BSM Higgs bosons. The pseudoscalar boson decays only into the fermionic sector: neither light  $M_A (\lesssim 38 \text{ GeV})$  nor approximately degenerate  $M_A$  with  $M_{H, H^\pm}$  in the PDG-island can accommodate the bosonic decays of  $A \rightarrow H^\pm W^{\pm(*)}/HZ^{(*)}$ . Furthermore, the suppressed couplings of  $A$  to the quark sector by large  $t_\beta$  make  $A \rightarrow \tau^+ \tau^-$  dominant [109,130]: its branching ratio is almost 100%. Another interesting decay channel is  $A \rightarrow \mu^+ \mu^-$ . Although it has a small branching ratio of about 0.3%, the absence of neutrinos helps reconstruct the pseudoscalar mass. On the other hand,  $H^\pm$  and  $H$  can have the bosonic decay modes of  $H^\pm \rightarrow W^\pm A$  and  $H \rightarrow ZA$  for light  $M_A$ . Since their partial decay widths are enhanced by a factor of  $(M_{H^\pm}^2/m_W^2)^2$  and  $(M_H^2/m_Z^2)^2$  respectively,  $H^\pm \rightarrow W^\pm A$  and  $H \rightarrow ZA$  are dominant in the mainland regions.

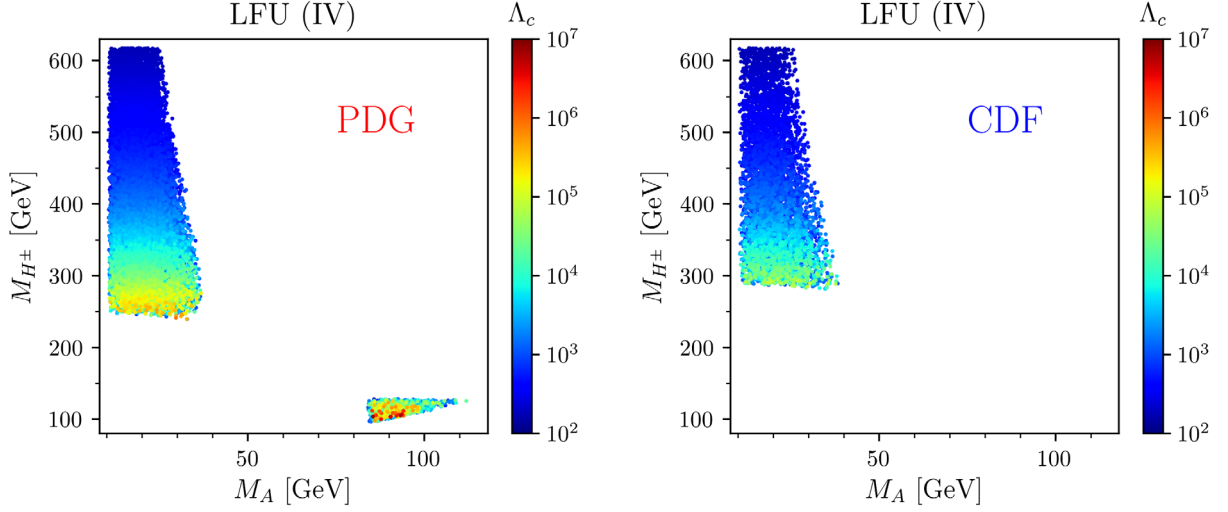


FIG. 9. Cutoff scales via the color code in the finally allowed  $(M_A, M_{H^\pm})$ . The left (right) shows the results in the PDG (CDF) case.

In Fig. 10, we present the branching ratios of  $H^\pm$  (left) and  $H$  (right) in the PDG (upper) and CDF cases (lower) over the finally allowed parameter points. The results of the PDG-island correspond to separate groups of the points for the light  $M_{H^\pm}/M_H$  in the upper panels. In the PDG-island,  $H^\pm \rightarrow \tau\nu$  and  $H \rightarrow \tau^+\tau^-$  have almost 100% branching

ratios. The muon modes,  $H^\pm \rightarrow \mu\nu$  and  $H \rightarrow \mu^+\mu^-$ , have about 0.3% branching ratios, which are omitted to avoid congestion. In the PDG-island, the bosonic decay modes are extremely suppressed such that  $\mathcal{B}(H^\pm \rightarrow AW^*) \lesssim 1.1 \times 10^{-5}$  and  $\mathcal{B}(H \rightarrow AZ^*) \lesssim 3.5 \times 10^{-5}$ . In the mainland regions of the PDG and CDF cases, the bosonic decay

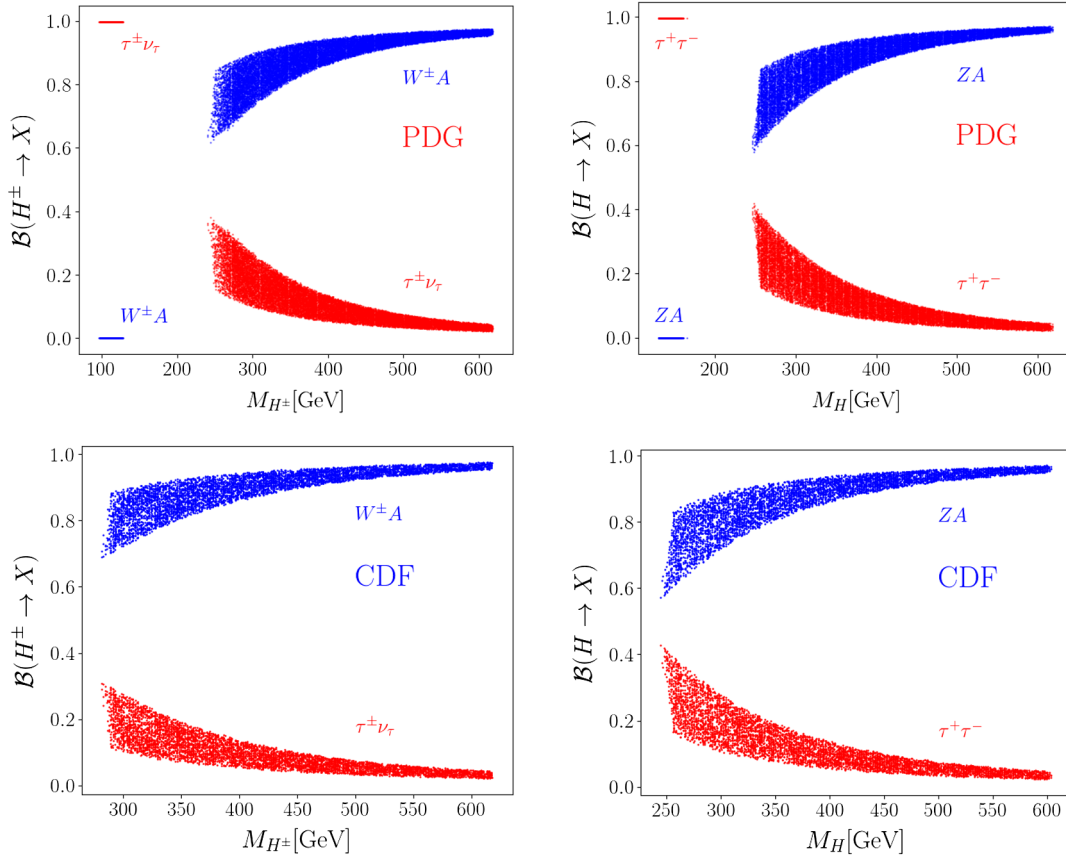


FIG. 10. Branching ratios of  $H^\pm$  (left panels) and  $H$  (right panels) in the PDG (upper panels) and CDF cases (lower panels), over the parameter points at the final step IV. The muon modes are not shown for simplicity.

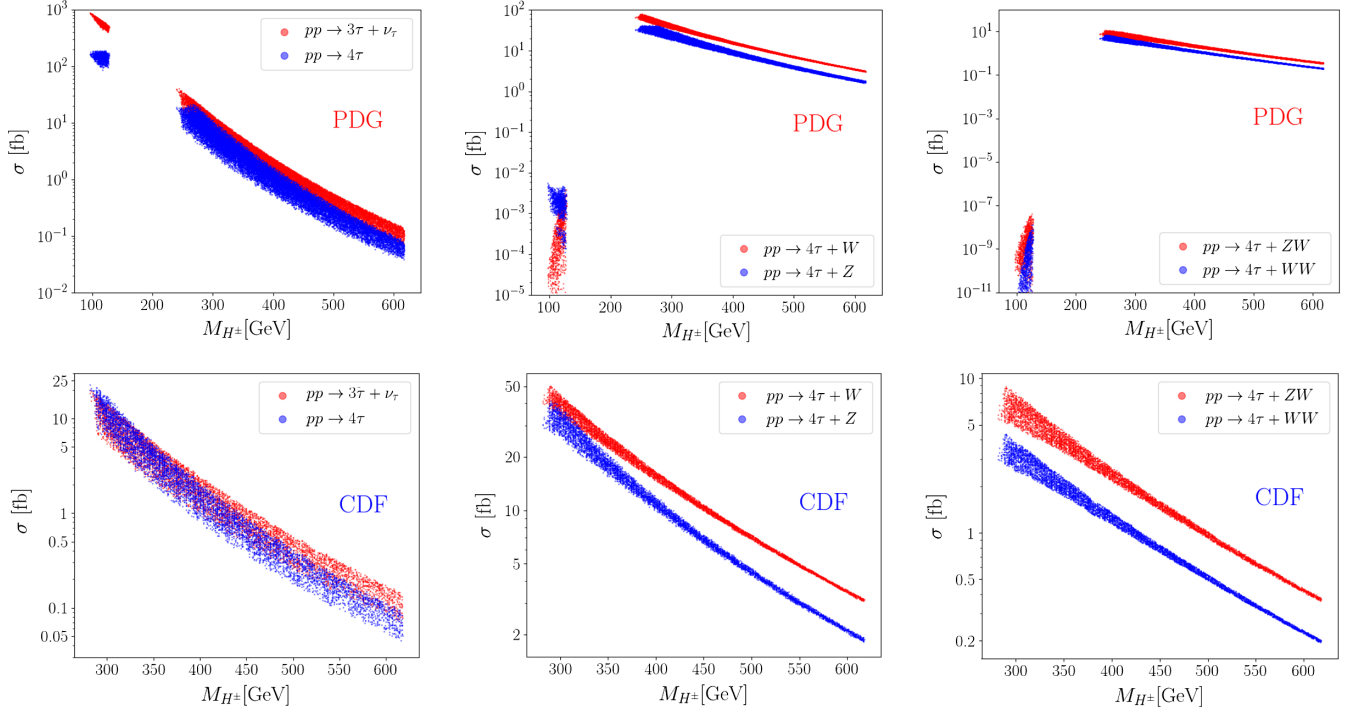


FIG. 11. Production cross-sections of multi- $\tau$  states as a function of  $M_{H^\pm}$ :  $3\tau/4\tau$  (left),  $4\tau + W(Z)$  (middle), and  $4\tau + ZW(WW)$  (right). The PDG (CDF) results are in the upper (lower) panels.

modes of  $H^\pm$  and  $H$  are dominant over the leptonic modes. The minimum of  $\mathcal{B}(H^\pm \rightarrow W^\pm A)$  is about 60% (70%) in the PDG (CDF) case. And  $\mathcal{B}(H \rightarrow ZA)$  is above about 60% in both the PDG and CDF cases.

Based on the branching ratios, we study the multi- $\tau$  states through the electroweak processes. First,  $3\tau + \nu$  states are from

$$\begin{aligned} 3\tau + \nu: \quad & pp \rightarrow H^\pm A \rightarrow [\tau^\pm \nu_\tau][\tau^+ \tau^-], \\ & pp \rightarrow H^\pm H \rightarrow [\tau^\pm \nu_\tau][\tau^+ \tau^-]. \end{aligned} \quad (32)$$

The  $4\tau$  states consist of

$$4\tau: \quad pp \rightarrow HA \rightarrow [\tau^+ \tau^-][\tau^+ \tau^-], \quad (33)$$

$$\begin{aligned} 4\tau + V: \quad & pp \rightarrow H^\pm A \rightarrow [W^\pm A]A \rightarrow [W^\pm \tau^+ \tau^-][\tau^+ \tau^-], \\ & pp \rightarrow HA \rightarrow [ZA]A \rightarrow [Z\tau^+ \tau^-][\tau^+ \tau^-], \end{aligned} \quad (34)$$

$$\begin{aligned} 4\tau + VV': \quad & pp \rightarrow H^\pm H \rightarrow [W^\pm A][ZA] \rightarrow [W\tau^+ \tau^-][Z\tau^+ \tau^-], \\ & pp \rightarrow H^+ H^- \rightarrow [W^+ A][W^- A] \\ & \rightarrow [W^+ \tau^+ \tau^-][W^- \tau^+ \tau^-], \end{aligned} \quad (35)$$

where  $V^{(\prime)} = Z, W^\pm$ . The production of  $HA$  ( $H^\pm A$ ), mediated by  $Z$  ( $W^\pm$ ), is favored by the Higgs alignment because the vertex of  $Z-H-A$  ( $W^\pm-H^\pm-A$ ) is proportional to  $s_{\beta-\alpha}$ .

To calculate the production cross sections of the multi- $\tau$  states, we first implement the type-X 2HDM in

FEYNRULES [131] to obtain the universal FeynRules output (UFO) [132]. Interfering the UFO file with MADGRAPH5-AMC@NLO [133], we compute the cross-sections of  $pp \rightarrow H^\pm A/H^\pm H/HA/H^+ H^-$  at 14 TeV LHC using NNPDF31\_LO\_AS\_0118 [134] parton distribution function set. The two-body cross sections are multiplied by relevant branching ratios of  $A, H^\pm$  and  $H$  from the 2HDMC [122].<sup>4</sup>

Figure 11 presents the parton level cross-sections of  $3\tau$  and  $4\tau$  states in Eqs. (32) and (33). We compare the PDG results (upper panels) with the CDF results (lower panels). The left panels show the cross-sections of the  $3\tau$  and  $4\tau$  states without a gauge boson. In the middle (right) panels, we show the cross-sections of  $4\tau + V$  ( $4\tau + VV'$ ). The PDG-island, which corresponds to  $M_{H^\pm} \lesssim 128$  GeV in the upper panels, shows different behaviors: the cross sections of  $3\tau$  and  $4\tau$  are substantially large, of the order of 1 pb and 100 fb respectively; the cross sections of  $4\tau + V$  and  $4\tau + VV'$  are highly suppressed like  $\sigma(pp \rightarrow 4\tau + VV') \lesssim 10^{-7}$  fb. It is attributed to the similar masses of BSM Higgs bosons as in Eq. (26), which suppress the bosonic decays. So,  $3\tau$  and  $4\tau$  states are the golden modes for the PDG-island. On the other hand, the PDG-mainland yields a similar signal rates to the CDF. The cross sections of  $4\tau + V$  is several times larger than those of  $3\tau/4\tau$  due to the dominant bosonic decays of  $H^\pm$  and  $H$ .

<sup>4</sup>The 2HDM UFO file in the MADGRAPH misses some important decay modes of BSM scalar bosons such as  $H^\pm \rightarrow cs$  and  $A \rightarrow gg$ .

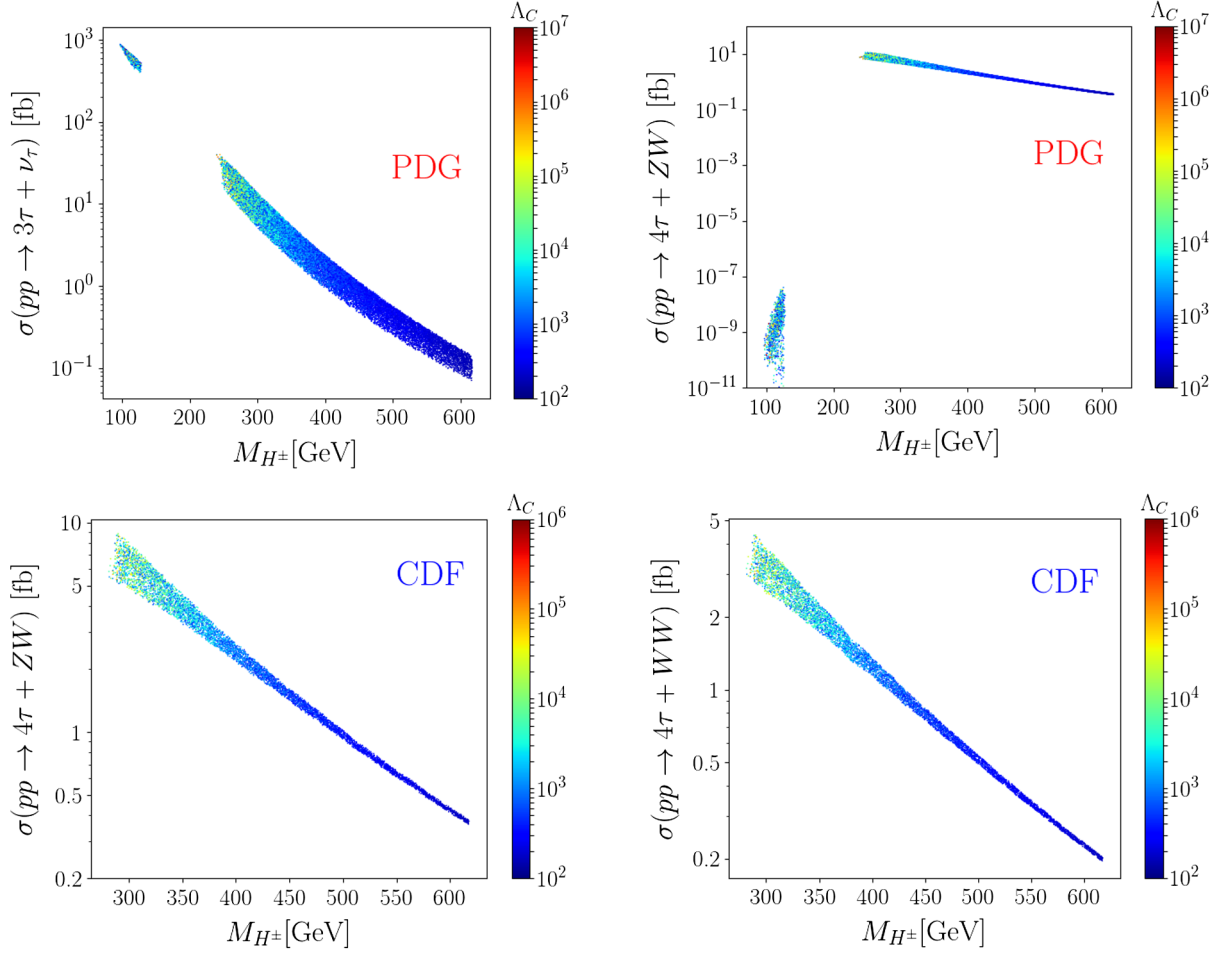


FIG. 12. The correlation between the cutoff scale  $\Lambda_c$  and the signal rates. In the PDG case, we present  $\sigma(pp \rightarrow 3\tau + \nu)$  in the upper-left panel and  $\sigma(pp \rightarrow 4\tau + ZW)$  in the upper-right panel, as a function of  $M_{H^\pm}$ . In the CDF case, we show  $\sigma(pp \rightarrow 4\tau + ZW)$  in the lower-left panel and  $\sigma(pp \rightarrow 4\tau + WW)$  in the lower-right panel. The color codes indicate the cutoff scale  $\Lambda_c$ .

The cross-sections of  $4\tau + VV'$  are a few times smaller than those of  $4\tau + V$ .

Now we discuss the correlation of the signal rates to the cutoff scales. Among six processes in Eqs. (33), (34), and (35), we concentrate on  $3\tau + \nu$  and  $4\tau + ZW$  for the PDG case while  $4\tau + ZW$  and  $4\tau + WW$  for the CDF case. The  $3\tau + \nu$  state targets the PDG-island. In Fig. 12, we present the cross sections as a function of  $M_{H^\pm}$  with the color code indicating  $\Lambda_c$ . The PDG results are in the upper panels, and the CDF results are in the lower panels. The color codes clearly show that all four processes have maximal signal rates when the cutoff scale is large. This correlation to  $\Lambda_c$  has a remarkable implication on the LHC phenomenology, such that the more valid the model is, the higher the discovery potential at the LHC is.

Based on the results in Figs. 11 and 12, we propose  $4\tau + VV'$  as the golden channel to probe the Higgs-ophobic type-X. First, the process, if observed at the HL-LHC, can exclude the PDG-island. The second merit is that the higher cutoff scale guarantees the larger cross section. The most

important merit of  $4\tau + VV'$  is almost background-free environment. For the irreducible backgrounds, we calculate the parton level cross sections of  $4\tau + ZW^\pm$  and  $4\tau + W^+W^-$  in the SM by using the MADGRAPH5-AMC@NLO [133]. We minimally impose the kinematic cuts on  $\tau$  as  $p_T^\tau > 10$  GeV,  $|\eta_\tau| < 2.5$ , and  $\Delta R(\tau, \tau) > 0.4$ . The SM cross sections are  $\sigma(pp \rightarrow 4\tau + ZW^\pm) \simeq 0.26$  ab and  $\sigma(pp \rightarrow 4\tau + W^+W^-) \simeq 0.54$  ab, which are negligible. Reducible backgrounds are the production of four QCD jets plus  $ZW^\pm$  or  $W^+W^-$ , where the QCD jets are misidentified as hadronically decaying tau lepton,  $\tau_h$ . Considering the mistagging rates of  $P_{j \rightarrow \tau_h} = 0.02$  in the one-prong decays and  $P_{j \rightarrow \tau_h} = 0.01$  in the three-prong decays, it is hard for the QCD jets to mimic the  $4\tau$  states. In addition, the large missing transverse energy cut additionally helps to tame the QCD jet backgrounds. Other possible reducible backgrounds would be  $t\bar{t} + \text{jets}$ ,  $V + \text{jets}$ , and  $VV' + \text{jets}$ . We can significantly reduce  $V(V') + \text{jets}$  backgrounds by imposing the selection cuts like  $n_\ell \geq 2$  and

$n_{\tau_h} \geq 4$ , where  $\ell = e, \mu$ . In addition to that, the  $b$ -veto will kill the  $t\bar{t} + \text{jets}$  background.

Nevertheless, there are concerns about the tau tagging. Due to the low mass of  $A$  and the decay chains involving  $W^\pm$  and  $Z$ , the  $\tau$ -jets will be soft, which results in a low  $\tau$ -tagging efficiency. In that situation, an alternative would be to consider the mixed state like  $2\ell + 2\tau_h$  decay mode of  $4\tau$  [109]. Then the final state of  $2\ell + 2\tau_h + ZW^\pm (W^+W^-)$  with leptonic decays of  $Z$  and  $W^\pm$  results in five (four)  $\ell$ 's, of which the backgrounds are negligible. In the era of the new  $W$  boson mass and the persistent  $\Delta a_\mu$ , it is worth studying the feasibility of  $4\tau + VV'$  states at the high luminosity phase of LHC, which we leave for our future study.

## VI. CONCLUSIONS

The recent measurement of the  $W$  boson mass by the CDF collaboration requests new physics beyond the SM: the Peskin-Takeuchi parameters significantly deviate from the SM expectation like  $S_{\text{CDF}} = 0.15 \pm 0.08$  and  $T_{\text{CDF}} = 0.27 \pm 0.06$  with  $U = 0$ . Another anomaly from the muon anomalous magnetic moment has been around for some time. Type-X in the 2HDM is one of the most attractive solutions for the muon  $g-2$  via a light pseudoscalar boson. Since the ordinary type-X suffers from  $h \rightarrow AA$  and the lepton flavor universality data in the  $\tau$  and  $Z$  decays, we have proposed the Higgs-phobic pseudoscalar in type-X.

Through random scanning of the model parameters, we impose the theoretical and experimental constraints step by step: step I is for the muon  $g-2$  and theoretical stabilities; step II is for the oblique parameters before and after the CDF  $m_W$  measurement; step III applies the Higgs precision data and the direct search bounds at high energy colliders; step IV includes the global  $\chi^2$  fit to  $\Delta a_\mu$  and the LFU data. The most important consequence is that the Higgs-phobic type-X can explain not only  $m_W^{\text{CDF}}$  and  $\Delta a_\mu$  anomalies but also all the other constraints, including the LFU observables.

Our main results are summarized as follows:

1. The muon  $g-2$  anomaly requires light  $M_A$  and large  $t_\beta$ .
2. The PDG and CDF cases share some common features:
  - (i) The theoretical constraints and the electroweak oblique parameters put the upper bounds on  $M_{H,H^\pm} \lesssim 600$  GeV.
  - (ii) The LFU data plays the essential role in the curtailment of the parameter space, eliminating most of the region with  $M_A \gtrsim 38$  GeV and  $t_\beta \gtrsim 70$ .
3. There exist meaningful differences between the PDG and CDF cases:
  - (i) Only in the PDG case, a small region where  $M_A \simeq M_{H^\pm} \simeq M_H \simeq 100$  GeV survives to the last step, called the PDG-island.

- (ii) The PDG-island accommodates both the right-sign and wrong-sign tau lepton Yukawa coupling, while outside the PDG-island only the wrong-sign  $\tau$  Yukawa coupling is allowed.
  - (iii) The lower bound on  $M_{H^\pm}$  for  $M_A \lesssim 38$  GeV is different,  $M_{H^\pm} \gtrsim 250$  GeV in the PDG case but  $M_{H^\pm} \gtrsim 300$  GeV in the CDF case.
  - (iv) The cutoff scale in the PDG case can go higher than in the CDF case, the former up to  $10^7$  GeV and the latter to  $10^5$  GeV.
4. We propose the  $4\tau$  states associated with  $ZW$  or  $WW$  as the golden discovery modes at the LHC for the CDF case, because of the background-free environment.

## ACKNOWLEDGMENTS

The work of J. K., S. L., and J. S. is supported by the National Research Foundation of Korea, Grant No. NRF-2022R1A2C1007583. The work of P. S. was supported by the appointment to the JRG Program at the APCTP through the Science and Technology Promotion Fund and Lottery Fund of the Korean Government. This was also supported by the Korean Local Governments—Gyeongsangbuk-do Province and Pohang City.

## APPENDIX A: CONTRIBUTIONS TO $\Delta a_\mu$ IN TYPE-X

In the 2HDM, there exist two kinds of contributions to  $\Delta a_\mu$ , one-loop contributions and two-loop Barr-Zee contributions [105,106]. The one-loop contributions mediated by  $H$ ,  $A$ , and  $H^\pm$  are [167]

$$\Delta a_\mu^{1\text{-loop}} = \frac{G_F m_\mu^2}{4\pi^2 \sqrt{2}} \sum_\phi (\xi_\mu^\phi)^2 \rho_\phi^\mu f_\phi(\rho_\phi^\mu), \quad (\text{A1})$$

where  $\phi = \{H, A, H^\pm\}$  and  $\rho_j^i = m_i^2/m_j^2$ . The loop function  $f_\phi$  is

$$\begin{aligned} f_H(\rho) &= \int_0^1 dx \frac{x^2(2-x)}{1-x+\rho x^2}, \\ f_A(\rho) &= - \int_0^1 dx \frac{x^3}{1-x+\rho x^2}, \\ f_{H^\pm}(\rho) &= - \int_0^1 dx \frac{x(1-x)}{1-\rho(1-x)}. \end{aligned} \quad (\text{A2})$$

At two-loop level, dominant contributions are from the Barr-Zee type diagrams with heavy fermions in the loop, given by [105]

$$\Delta a_\mu^{\text{BZ}} = \frac{G_F m_\mu^2}{4\pi^2 \sqrt{2}} \frac{\alpha_{\text{em}}}{\pi} \sum_{f,\phi^0} N_f^c Q_f^2 \xi_\mu^{\phi^0} \xi_f^{\phi^0} \rho_{\phi^0}^f g_{\phi^0}^f(\rho_{\phi^0}^f), \quad (\text{A3})$$

where  $f = t, b, \tau$ ,  $\phi^0 = H, A$ ,  $m_f$ ,  $Q_f$  and  $N_f^c$  are the mass, electric charge and color factor of the fermion  $f$ . The loop functions are

$$\begin{aligned} g_H(\rho) &= \int_0^1 dx \frac{2x(1-x) - 1}{x(1-x) - \rho} \ln \frac{x(1-x)}{\rho}, \\ g_A(\rho) &= \int_0^1 dx \frac{1}{x(1-x) - \rho} \ln \frac{x(1-x)}{\rho}. \end{aligned} \quad (\text{A4})$$

For light  $M_A$  and  $t_\beta \gtrsim 30$ , the largest contribution is from the Barr-Zee diagram with  $\tau$  loop, mediated by  $A$ .

## APPENDIX B: LEPTON FLAVOR UNIVERSALITY OBSERVABLES IN THE 2HDM

For the HFLAV global fit results in the  $\tau$  decay, the coupling ratios in the 2HDM are<sup>5</sup>

$$\begin{aligned} \frac{g_\tau}{g_\mu} &= \left( \frac{g_\tau}{g_\mu} \right)_\pi = \left( \frac{g_\tau}{g_\mu} \right)_K = 1 + \delta_{\text{loop}}, \\ \frac{g_\tau}{g_e} &= 1 + \delta_{\text{loop}} + \epsilon_{\text{tree}}^\tau, \end{aligned} \quad (\text{B1})$$

$$\frac{g_\mu}{g_e} = 1 + \epsilon_{\text{tree}}^\tau, \quad (\text{B2})$$

where  $\delta_{\text{loop}}$  and  $\epsilon_{\text{tree}}^\tau$  are

$$\delta_{\text{loop}} = \frac{1}{16\pi^2} \frac{m_\tau^2 t_\beta^2}{v^2} \left[ 1 + \frac{1}{4} \{k(\rho_{H^\pm}^A) + k(\rho_{H^\pm}^H)\} \right], \quad (\text{B3})$$

$$\epsilon_{\text{tree}}^\tau = \delta_{\text{tree}} \left[ \frac{\delta_{\text{tree}}}{8} - \frac{m_\mu}{m_\tau} \frac{g(\rho_\tau^\mu)}{f(\rho_\tau^\mu)} \right]. \quad (\text{B4})$$

<sup>5</sup>Equation (29) in Ref. [103] has a typo. The correct one is  $\mathcal{R}_{1,2,3}^\tau = 1 + \delta_{\text{loop}}$ .

The expression in Eq. (B3) is valid in the Higgs alignment limit, which is almost maintained in our model. Here  $\delta_{\text{tree}}$  denotes the generic tree-level contribution mediated by the charged Higgs boson, given by

$$\delta_{\text{tree}} = \frac{m_\mu m_\tau t_\beta^2}{M_{H^\pm}^2}. \quad (\text{B5})$$

The loop functions in Eq. (B3) and Eq. (B4) are

$$\begin{aligned} k(x) &= (1+x) \ln x/(1-x), \\ g(x) &= 1 + 9x - 9x^2 - x^3 + 6x(1+x) \ln x, \\ f(x) &= 1 - 8x + 8x^3 - x^4 - 12x^2 \ln x. \end{aligned} \quad (\text{B6})$$

Among the Michel parameters in Eq. (22), the 2HDM only affects  $\eta_\mu$ ,  $(\xi\delta)_\mu$ , and  $\xi_\mu$  as

$$\eta_\mu = -\frac{2\delta_{\text{tree}}(1 + \delta_{\text{loop}})}{4 + \delta_{\text{tree}}^2}, \quad (\text{B7})$$

$$(\xi\delta)_\mu = \frac{3}{4} \times \frac{4(1 + \delta_{\text{loop}})^2 - \delta_{\text{tree}}^2}{4(1 + \delta_{\text{loop}})^2 + \delta_{\text{tree}}^2}, \quad (\text{B8})$$

$$\xi_\mu = \frac{4(1 + \delta_{\text{loop}})^2 - \delta_{\text{tree}}^2}{4(1 + \delta_{\text{loop}})^2 + \delta_{\text{tree}}^2}. \quad (\text{B9})$$

And the new contributions to the leptonic  $Z$  decays are written as

$$\begin{aligned} &\frac{\Gamma(Z \rightarrow l^+ l^-)}{\Gamma(Z \rightarrow e^+ e^-)} - 1 \\ &= \frac{2g_L^{\text{SM}} \text{Re}(\delta g_L^l) + 2g_R^{\text{SM}} \text{Re}(\delta g_R^l)}{(g_L^{\text{SM}})^2 + (g_R^{\text{SM}})^2}, \quad (l = \mu, \tau) \end{aligned} \quad (\text{B10})$$

where  $g_L^{\text{SM}} = s_W^2 - 1/2$ ,  $g_R^{\text{SM}} = s_W^2$ , and the full expressions for  $\delta g_{L/R}^{\mu,\tau}$  at one-loop level are referred to Ref. [167].

[1] T. Aaltonen *et al.* (CDF Collaboration), High-precision measurement of the  $W$  boson mass with the CDF II detector, *Science* **376**, 170 (2022).  
[2] P. A. Zyla *et al.* (Particle Data Group), Review of particle physics, *Prog. Theor. Exp. Phys.* **2020**, 083C01 (2020).  
[3] M. Aaboud *et al.* (ATLAS Collaboration), Measurement of the  $W$ -boson mass in pp collisions at  $\sqrt{s} = 7$  TeV with the ATLAS detector, *Eur. Phys. J. C* **78**, 110 (2018).  
[4] C.-T. Lu, L. Wu, Y. Wu, and B. Zhu, Electroweak precision fit and new physics in light of  $W$  boson mass, [arXiv:2204.03796](https://arxiv.org/abs/2204.03796).

[5] P. Asadi, C. Cesarotti, K. Fraser, S. Homiller, and A. Parikh, Oblique lessons from the  $W$  mass measurement at CDF II, [arXiv:2204.05283](https://arxiv.org/abs/2204.05283).  
[6] R. Balkin, E. Madge, T. Menzo, G. Perez, Y. Soreq, and J. Zupan, On the implications of positive  $W$  mass shift, *J. High Energy Phys.* **05** (2022) 133.  
[7] A. Stumia, Interpreting electroweak precision data including the  $W$ -mass CDF anomaly, [arXiv:2204.04191](https://arxiv.org/abs/2204.04191).  
[8] J. de Blas, M. Pierini, L. Reina, and L. Silvestrini, Impact of the recent measurements of the top-quark and  $W$ -boson masses on electroweak precision fits, [arXiv:2204.04204](https://arxiv.org/abs/2204.04204).

- [9] Y.-Z. Fan, T.-P. Tang, Y.-L. S. Tsai, and L. Wu, Inert Higgs dark matter for new CDF  $W$ -boson mass and detection prospects, [arXiv:2204.03693](#).
- [10] C.-R. Zhu, M.-Y. Cui, Z.-Q. Xia, Z.-H. Yu, X. Huang, Q. Yuan *et al.*, GeV antiproton/gamma-ray excesses and the  $W$ -boson mass anomaly: three faces of  $\sim 60$ – $70$  GeV dark matter particle?, [arXiv:2204.03767](#).
- [11] B.-Y. Zhu, S. Li, J.-G. Cheng, R.-L. Li, and Y.-F. Liang, Using gamma-ray observation of dwarf spheroidal galaxy to test a dark matter model that can interpret the  $W$ -boson mass anomaly, [arXiv:2204.04688](#).
- [12] H. Song, W. Su, and M. Zhang, Electroweak phase transition in 2HDM under Higgs,  $Z$ -pole, and  $W$  precision measurements, [arXiv:2204.05085](#).
- [13] H. Bahl, J. Braathen, and G. Weiglein, New physics effects on the  $W$ -boson mass from a doublet extension of the SM Higgs sector, [arXiv:2204.05269](#).
- [14] Y. Heo, D.-W. Jung, and J. S. Lee, Impact of the CDF  $W$ -mass anomaly on two Higgs doublet model, [arXiv:2204.05728](#).
- [15] K. S. Babu, S. Jana, and P. K. Vishnu, Correlating  $W$ -boson mass shift with muon  $g - 2$  in the 2HDM, [arXiv:2204.05303](#).
- [16] T. Biekötter, S. Heinemeyer, and G. Weiglein, Excesses in the low-mass Higgs-boson search and the  $W$ -boson mass measurement, [arXiv:2204.05975](#).
- [17] Y. H. Ahn, S. K. Kang, and R. Ramos, Implications of new CDF-II  $W$  boson mass on two Higgs doublet model, [arXiv:2204.06485](#).
- [18] X.-F. Han, F. Wang, L. Wang, J. M. Yang, and Y. Zhang, A joint explanation of  $W$ -mass and muon  $g-2$  in 2HDM, [arXiv:2204.06505](#).
- [19] G. Arcadi and A. Djouadi, The 2HD+a model for a combined explanation of the possible excesses in the CDF  $M_W$  measurement and  $(g - 2)_\mu$  with dark matter, [arXiv:2204.08406](#).
- [20] K. Ghorbani and P. Ghorbani,  $W$ -boson mass anomaly from scale invariant 2HDM, [arXiv:2204.09001](#).
- [21] Y. Cheng, X.-G. He, Z.-L. Huang, and M.-W. Li, Type-II seesaw triplet scalar effects on neutrino trident scattering, *Phys. Lett. B* **831**, 137218 (2022).
- [22] X. K. Du, Z. Li, F. Wang, and Y. K. Zhang, Explaining the new CDF II  $W$ -boson mass data in the Georgi-Machacek extension models, [arXiv:2204.05760](#).
- [23] S. Kanemura and K. Yagyu, Implication of the  $W$  boson mass anomaly at CDF II in the Higgs triplet model with a mass difference, *Phys. Lett. B* **831**, 137217 (2022).
- [24] P. Mondal, Enhancement of the  $W$  boson mass in the Georgi-Machacek model, [arXiv:2204.07844](#).
- [25] D. Borah, S. Mahapatra, D. Nanda, and N. Sahu, Type II Dirac seesaw with observable  $\Delta N_{\text{eff}}$  in the light of  $W$ -mass anomaly, [arXiv:2204.08266](#).
- [26] J. M. Yang and Y. Zhang, Low energy SUSY confronted with new measurements of  $W$ -boson mass and muon  $g-2$ , [arXiv:2204.04202](#).
- [27] X. K. Du, Z. Li, F. Wang, and Y. K. Zhang, Explaining the muon  $g - 2$  anomaly and new CDF II  $W$ -boson mass in the framework of (extra)ordinary gauge mediation, [arXiv:2204.04286](#).
- [28] P. Athron, M. Bach, D. H. J. Jacob, W. Kotlarski, D. Stöckinger, and A. Voigt, Precise calculation of the  $W$  boson pole mass beyond the standard model with flexibleSUSY, [arXiv:2204.05285](#).
- [29] M.-D. Zheng, F.-Z. Chen, and H.-H. Zhang, The  $W\ell\nu$ -vertex corrections to  $W$ -boson mass in the R-parity violating MSSM, [arXiv:2204.06541](#).
- [30] A. Ghoshal, N. Okada, S. Okada, D. Raut, Q. Shafi, and A. Thapa, Type III seesaw with R-parity violation in light of  $m_W$  (CDF), [arXiv:2204.07138](#).
- [31] M. Blennow, P. Coloma, E. Fernández-Martínez, and M. González-López, Right-handed neutrinos and the CDF II anomaly, [arXiv:2204.04559](#).
- [32] F. Arias-Aragón, E. Fernández-Martínez, M. González-López, and L. Merlo, Dynamical minimal flavour violating inverse seesaw, [arXiv:2204.04672](#).
- [33] X. Liu, S.-Y. Guo, B. Zhu, and Y. Li, Unifying gravitational waves with  $W$  boson, FIMP dark matter, and Majorana Seesaw mechanism, [arXiv:2204.04834](#).
- [34] O. Popov and R. Srivastava, The triplet dirac seesaw in the view of the recent CDF-II  $W$  mass anomaly, [arXiv:2204.08568](#).
- [35] A. Crivellin, M. Kirk, T. Kitahara, and F. Mescia, Correlating  $t \rightarrow cZ$  to the  $W$  mass and  $B$  physics with vector-like quarks, [arXiv:2204.05962](#).
- [36] J. Fan, L. Li, T. Liu, and K.-F. Lyu,  $W$ -boson mass, electroweak precision tests and SMEFT, [arXiv:2204.04805](#).
- [37] E. Bagnaschi, J. Ellis, M. Madigan, K. Mimasu, V. Sanz, and T. You, SMEFT analysis of  $m_W$ , [arXiv:2204.05260](#).
- [38] A. Paul and M. Valli, Violation of custodial symmetry from  $W$ -boson mass measurements, [arXiv:2204.05267](#).
- [39] J. Gu, Z. Liu, T. Ma, and J. Shu, Speculations on the  $W$ -mass measurement at CDF, [arXiv:2204.05296](#).
- [40] L. Di Luzio, R. Gröber, and P. Paradisi, Higgs physics confronts the  $M_W$  anomaly, [arXiv:2204.05284](#).
- [41] M. Endo and S. Mishima, New physics interpretation of  $W$ -boson mass anomaly, [arXiv:2204.05965](#).
- [42] V. Cirigliano, W. Dekens, J. de Vries, E. Mereghetti, and T. Tong, Beta-decay implications for the  $W$ -boson mass anomaly, [arXiv:2204.08440](#).
- [43] G.-W. Yuan, L. Zu, L. Feng, Y.-F. Cai, and Y.-Z. Fan, Hint on new physics from the  $W$ -boson mass excess-axion-like particle, dark photon or Chameleon dark energy, [arXiv:2204.04183](#).
- [44] G. Cacciapaglia and F. Sannino, The  $W$  boson mass weighs in on the non-standard Higgs, *Phys. Lett. B* **832**, 137232 (2022).
- [45] K. Sakurai, F. Takahashi, and W. Yin, Singlet extensions and  $W$  boson mass in the light of the CDF II result, [arXiv:2204.04770](#).
- [46] J. J. Heckman, Extra  $W$ -boson mass from a D3-brane, [arXiv:2204.05302](#).
- [47] N. V. Krasnikov, Nonlocal generalization of the SM as an explanation of recent CDF result, [arXiv:2204.06327](#).
- [48] Z. Péli and Z. Trócsányi, Vacuum stability and scalar masses in the superweak extension of the standard model, [arXiv:2204.07100](#).
- [49] P. Fileviez Perez, H. H. Patel, and A. D. Plascencia, On the  $W$ -mass and new Higgs bosons, [arXiv:2204.07144](#).

- [50] R. A. Wilson, A toy model for the  $W/Z$  mass ratio, [arXiv:2204.07970](#).
- [51] K.-Y. Zhang and W.-Z. Feng, Explaining  $W$  boson mass anomaly and dark matter with a  $U(1)$  dark sector, [arXiv:2204.08067](#).
- [52] L. M. Carpenter, T. Murphy, and M. J. Smylie, Changing patterns in electroweak precision with new color-charged states: Oblique corrections and the  $W$  boson mass, [arXiv:2204.08546](#).
- [53] M. Du, Z. Liu, and P. Nath, CDF  $W$  mass anomaly from a dark sector with a Stueckelberg-Higgs portal, [arXiv:2204.09024](#).
- [54] S. Lee, K. Cheung, J. Kim, C.-T. Lu, and J. Song, Status of the two-Higgs-doublet model in light of the CDF  $m_W$  measurement, [arXiv:2204.10338](#).
- [55] T.-K. Chen, C.-W. Chiang, and K. Yagyu, Explanation of the  $W$  mass shift at CDF II in the Georgi-Machacek Model, [arXiv:2204.12898](#).
- [56] J. Cao, L. Meng, L. Shang, S. Wang, and B. Yang, Interpreting the  $W$  mass anomaly in the vectorlike quark models, [arXiv:2204.09477](#).
- [57] H. Abouabid, A. Arhrib, R. Benbrik, M. Krab, and M. Ouchemhou, Is the new CDF  $M_W$  measurement consistent with the two Higgs doublet model?, [arXiv:2204.12018](#).
- [58] B. Abi *et al.* (Muon  $g-2$  Collaboration), Measurement of the Positive Muon Anomalous Magnetic Moment to 0.46 ppm, *Phys. Rev. Lett.* **126**, 141801 (2021).
- [59] T. Albahri *et al.* (Muon  $g-2$  Collaboration), Measurement of the anomalous precession frequency of the muon in the Fermilab Muon  $g-2$  Experiment, *Phys. Rev. D* **103**, 072002 (2021).
- [60] G. W. Bennett *et al.* (Muon  $g-2$  Collaboration), Final report of the muon E821 anomalous magnetic moment measurement at BNL, *Phys. Rev. D* **73**, 072003 (2006).
- [61] T. Aoyama, M. Hayakawa, T. Kinoshita, and M. Nio, Complete Tenth-Order QED Contribution to the Muon  $g-2$ , *Phys. Rev. Lett.* **109**, 111808 (2012).
- [62] T. Aoyama, T. Kinoshita, and M. Nio, Theory of the anomalous magnetic moment of the electron, *Atoms* **7**, 28 (2019).
- [63] A. Czarnecki, W. J. Marciano, and A. Vainshtein, Refinements in electroweak contributions to the muon anomalous magnetic moment, *Phys. Rev. D* **67**, 073006 (2003).
- [64] C. Gnendiger, D. Stöckinger, and H. Stöckinger-Kim, The electroweak contributions to  $(g-2)_\mu$  after the Higgs boson mass measurement, *Phys. Rev. D* **88**, 053005 (2013).
- [65] M. Davier, A. Hoecker, B. Malaescu, and Z. Zhang, Reevaluation of the hadronic vacuum polarisation contributions to the Standard Model predictions of the muon  $g-2$  and  $\alpha(m_Z^2)$  using newest hadronic cross-section data, *Eur. Phys. J. C* **77**, 827 (2017).
- [66] A. Keshavarzi, D. Nomura, and T. Teubner, Muon  $g-2$  and  $\alpha(M_Z^2)$ : A new data-based analysis, *Phys. Rev. D* **97**, 114025 (2018).
- [67] G. Colangelo, M. Hoferichter, and P. Stoffer, Two-pion contribution to hadronic vacuum polarization, *J. High Energy Phys.* **02** (2019) 006.
- [68] M. Hoferichter, B.-L. Hoid, and B. Kubis, Three-pion contribution to hadronic vacuum polarization, *J. High Energy Phys.* **08** (2019) 137.
- [69] M. Davier, A. Hoecker, B. Malaescu, and Z. Zhang, A new evaluation of the hadronic vacuum polarisation contributions to the muon anomalous magnetic moment and to  $\alpha(m_Z^2)$ , *Eur. Phys. J. C* **80**, 241 (2020).
- [70] A. Keshavarzi, D. Nomura, and T. Teubner,  $g-2$  of charged leptons,  $\alpha(M_Z^2)$ , and the hyperfine splitting of muonium, *Phys. Rev. D* **101**, 014029 (2020).
- [71] A. Kurz, T. Liu, P. Marquard, and M. Steinhauser, Hadronic contribution to the muon anomalous magnetic moment to next-to-next-to-leading order, *Phys. Lett. B* **734**, 144 (2014).
- [72] K. Melnikov and A. Vainshtein, Hadronic light-by-light scattering contribution to the muon anomalous magnetic moment revisited, *Phys. Rev. D* **70**, 113006 (2004).
- [73] P. Masjuan and P. Sanchez-Puertas, Pseudoscalar-pole contribution to the  $(g_\mu - 2)$ : A rational approach, *Phys. Rev. D* **95**, 054026 (2017).
- [74] G. Colangelo, M. Hoferichter, M. Procura, and P. Stoffer, Dispersion relation for hadronic light-by-light scattering: Two-pion contributions, *J. High Energy Phys.* **04** (2017) 161.
- [75] M. Hoferichter, B.-L. Hoid, B. Kubis, S. Leupold, and S. P. Schneider, Dispersion relation for hadronic light-by-light scattering: Pion pole, *J. High Energy Phys.* **10** (2018) 141.
- [76] A. Gérardin, H. B. Meyer, and A. Nyffeler, Lattice calculation of the pion transition form factor with  $N_f = 2 + 1$  Wilson quarks, *Phys. Rev. D* **100**, 034520 (2019).
- [77] J. Bijnens, N. Hermansson-Truedsson, and A. Rodríguez-Sánchez, Short-distance constraints for the HLbL contribution to the muon anomalous magnetic moment, *Phys. Lett. B* **798**, 134994 (2019).
- [78] G. Colangelo, F. Hagelstein, M. Hoferichter, L. Laub, and P. Stoffer, Longitudinal short-distance constraints for the hadronic light-by-light contribution to  $(g-2)_\mu$  with large- $N_c$  Regge models, *J. High Energy Phys.* **03** (2020) 101.
- [79] T. Blum, N. Christ, M. Hayakawa, T. Izubuchi, L. Jin, C. Jung, and C. Lehner, Hadronic Light-by-Light Scattering Contribution to the Muon Anomalous Magnetic Moment from Lattice QCD, *Phys. Rev. Lett.* **124**, 132002 (2020).
- [80] G. Colangelo, M. Hoferichter, A. Nyffeler, M. Passera, and P. Stoffer, Remarks on higher-order hadronic corrections to the muon  $g-2$ , *Phys. Lett. B* **735**, 90 (2014).
- [81] T. Aoyama *et al.*, The anomalous magnetic moment of the muon in the Standard Model, *Phys. Rep.* **887**, 1 (2020).
- [82] H. M. Lee and K. Yamashita, A model of vector-like leptons for the muon  $g-2$  and the  $W$  boson mass, [arXiv:2204.05024](#).
- [83] S. Baek, Implications of CDF  $W$ -mass and  $(g-2)_\mu$  on  $U(1)_{L_\mu-L_\tau}$  model, [arXiv:2204.09585](#).
- [84] Q. Zhou and X.-F. Han, The CDF  $W$ -mass, muon  $g-2$ , and dark matter in a  $U(1)_{L_\mu-L_\tau}$  model with vector-like leptons, [arXiv:2204.13027](#).
- [85] K. Cheung, W.-Y. Keung, and P.-Y. Tseng, Iso-doublet vector leptoquark solution to the muon  $g-2$ ,  $R_{K,K^*}$ ,  $R_{D,D^*}$ , and  $W$ -mass anomalies, [arXiv:2204.05942](#).
- [86] A. Bhaskar, A. A. Madathil, T. Mandal, and S. Mitra, Combined explanation of  $W$ -mass, muon  $g-2$ ,  $R_{K^{(*)}}$  and  $R_{D^{(*)}}$  anomalies in a singlet-triplet scalar leptoquark model, [arXiv:2204.09031](#).



- [87] P. Athron, A. Fowlie, C.-T. Lu, L. Wu, Y. Wu, and B. Zhu, The  $W$  boson mass and muon  $g - 2$ : Hadronic uncertainties or new physics?, [arXiv:2204.03996](#).
- [88] T. A. Chowdhury, J. Heeck, S. Saad, and A. Thapa,  $W$  boson mass shift and muon magnetic moment in the Zee model, [arXiv:2204.08390](#).
- [89] J. Kawamura, S. Okawa, and Y. Omura,  $W$  boson mass and muon  $g - 2$  in a lepton portal dark matter model, [arXiv:2204.07022](#).
- [90] K. I. Nagao, T. Nomura, and H. Okada, A model explaining the new CDF II  $W$  boson mass linking to muon  $g - 2$  and dark matter, [arXiv:2204.07411](#).
- [91] F. J. Botella, F. Cornet-Gomez, C. Miró, and M. Nebot, Muon and electron  $g - 2$  anomalies in a flavor conserving 2HDM with an oblique view on the CDF  $M_W$  value, [arXiv:2205.01115](#).
- [92] T.-P. Tang, M. Abdughani, L. Feng, Y.-L. S. Tsai, J. Wu, and Y.-Z. Fan, NMSSM neutralino dark matter for  $W$ -boson mass and muon  $g - 2$  and the promising prospect of direct detection, [arXiv:2204.04356](#).
- [93] T. Abe, R. Sato, and K. Yagyu, Lepton-specific two Higgs doublet model as a solution of muon  $g - 2$  anomaly, *J. High Energy Phys.* **07** (2015) 064.
- [94] T. Han, S. K. Kang, and J. Sayre, Muon  $g - 2$  in the aligned two Higgs doublet model, *J. High Energy Phys.* **02** (2016) 097.
- [95] A. Cherchiglia, P. Kneschke, D. Stöckinger, and H. Stöckinger-Kim, The muon magnetic moment in the 2HDM: Complete two-loop result, *J. High Energy Phys.* **01** (2017) 007.
- [96] A. Cherchiglia, D. Stöckinger, and H. Stöckinger-Kim, Muon  $g-2$  in the 2HDM: Maximum results and detailed phenomenology, *Phys. Rev. D* **98**, 035001 (2018).
- [97] X.-F. Han, T. Li, L. Wang, and Y. Zhang, Simple interpretations of lepton anomalies in the lepton-specific inert two-Higgs-doublet model, *Phys. Rev. D* **99**, 095034 (2019).
- [98] L. Wang, J. M. Yang, M. Zhang, and Y. Zhang, Revisiting lepton-specific 2HDM in light of muon  $g - 2$  anomaly, *Phys. Lett. B* **788**, 519 (2019).
- [99] E. J. Chun, J. Kim, and T. Mondal, Electron EDM and muon anomalous magnetic moment in two-Higgs-doublet models, *J. High Energy Phys.* **12** (2019) 068.
- [100] L. Delle Rose, S. Khalil, and S. Moretti, Explaining electron and muon  $g - 2$  anomalies in an Aligned 2-Higgs doublet model with right-handed neutrinos, *Phys. Lett. B* **816**, 136216 (2021).
- [101] S. Jana, V. P. K., and S. Saad, Resolving electron and muon  $g - 2$  within the 2HDM, *Phys. Rev. D* **101**, 115037 (2020).
- [102] N. Ghosh and J. Lahiri, Revisiting a generalized two-Higgs-doublet model in light of the muon anomaly and lepton flavor violating decays at the HL-LHC, *Phys. Rev. D* **103**, 055009 (2021).
- [103] A. Jueid, J. Kim, S. Lee, and J. Song, Type-X two-Higgs-doublet model in light of the muon  $g-2$ : Confronting Higgs boson and collider data, *Phys. Rev. D* **104**, 095008 (2021).
- [104] P. Athron, C. Balazs, A. Cherchiglia, D. H. J. Jacob, D. Stöckinger, H. Stöckinger-Kim, and A. Voigt, Two-loop prediction of the anomalous magnetic moment of the muon in the two-Higgs doublet model with GM2Calc 2, *Eur. Phys. J. C* **82**, 229 (2022).
- [105] S. M. Barr and A. Zee, Electric Dipole Moment of the Electron and of the Neutron, *Phys. Rev. Lett.* **65**, 21 (1990).
- [106] V. Ilisie, New Barr-Zee contributions to  $(g - 2)_\mu$  in two-Higgs-doublet models, *J. High Energy Phys.* **04** (2015) 077.
- [107] A. M. Sirunyan *et al.* (CMS Collaboration), Search for an exotic decay of the Higgs boson to a pair of light pseudoscalars in the final state of two muons and two  $\tau$  leptons in proton-proton collisions at  $\sqrt{s} = 13$  TeV, *J. High Energy Phys.* **11** (2018) 018.
- [108] K. Cheung, A. Jueid, J. Kim, S. Lee, C.-T. Lu, and J. Song, Comprehensive study of the light charged Higgs boson in the type-I two-Higgs-doublet model, *Phys. Rev. D* **105**, 095044 (2022).
- [109] S. Kanemura, K. Tsumura, and H. Yokoya, Multi-tau-lepton signatures at the LHC in the two Higgs doublet model, *Phys. Rev. D* **85**, 095001 (2012).
- [110] E. J. Chun, S. Dwivedi, T. Mondal, and B. Mukhopadhyaya, Reconstructing a light pseudoscalar in the Type-X Two Higgs Doublet Model, *Phys. Lett. B* **774**, 20 (2017).
- [111] S. Kanemura, M. Takeuchi, and K. Yagyu, Probing double-aligned two-Higgs-doublet models at the LHC, *Phys. Rev. D* **105**, 115001 (2022).
- [112] E. J. Chun, Z. Kang, M. Takeuchi, and Y.-L. S. Tsai, LHC  $\tau$ -rich tests of lepton-specific 2HDM for  $(g-2)$ , *J. High Energy Phys.* **11** (2015) 099.
- [113] G. C. Branco, P. M. Ferreira, L. Lavoura, M. N. Rebelo, M. Sher, and J. P. Silva, Theory and phenomenology of two-Higgs-doublet models, *Phys. Rep.* **516**, 1 (2012).
- [114] S. L. Glashow and S. Weinberg, Natural conservation laws for neutral currents, *Phys. Rev. D* **15**, 1958 (1977).
- [115] E. A. Paschos, Diagonal neutral currents, *Phys. Rev. D* **15**, 1966 (1977).
- [116] J. Song and Y. W. Yoon,  $W\gamma$  decay of the elusive charged Higgs boson in the two-Higgs-doublet model with vector-like fermions, *Phys. Rev. D* **100**, 055006 (2019).
- [117] G. Aad *et al.* (ATLAS Collaboration), Combined measurements of Higgs boson production and decay using up to  $80 \text{ fb}^{-1}$  of proton-proton collision data at  $\sqrt{s} = 13$  TeV collected with the ATLAS experiment, *Phys. Rev. D* **101**, 012002 (2020).
- [118] A. M. Sirunyan *et al.* (CMS Collaboration), Evidence for Higgs boson decay to a pair of muons, *J. High Energy Phys.* **01** (2021) 148.
- [119] ATLAS Collaboration, Combined measurements of Higgs boson production and decay using up to  $139 \text{ fb}^{-1}$  of proton-proton collision data at  $\sqrt{s} = 13$  TeV collected with the ATLAS experiment, Report No. ATLAS-CONF-2021-053.
- [120] S. Chang, S. K. Kang, J.-P. Lee, and J. Song, Higgs potential and hidden light Higgs scenario in two Higgs doublet models, *Phys. Rev. D* **92**, 075023 (2015).
- [121] D. Das and I. Saha, Search for a stable alignment limit in two-Higgs-doublet models, *Phys. Rev. D* **91**, 095024 (2015).

- [122] D. Eriksson, J. Rathsman, and O. Stal, 2HDMC: Two-Higgs-doublet model calculator physics and manual, *Comput. Phys. Commun.* **181**, 189 (2010).
- [123] P. Bechtle, S. Heinemeyer, T. Klingl, T. Stefaniak, G. Weiglein, and J. Wittbrodt, HiggsSignals-2: Probing new physics with precision Higgs measurements in the LHC 13 TeV era, *Eur. Phys. J. C* **81**, 145 (2021).
- [124] P. Bechtle, D. Dercks, S. Heinemeyer, T. Klingl, T. Stefaniak, G. Weiglein, and J. Wittbrodt, HiggsBounds-5: Testing Higgs sectors in the LHC 13 TeV era, *Eur. Phys. J. C* **80**, 1211 (2020).
- [125] P. M. Ferreira, J. F. Gunion, H. E. Haber, and R. Santos, Probing wrong-sign Yukawa couplings at the LHC and a future linear collider, *Phys. Rev. D* **89**, 115003 (2014).
- [126] N. M. Coyle, B. Li, and C. E. M. Wagner, Wrong sign bottom Yukawa coupling in low energy supersymmetry, *Phys. Rev. D* **97**, 115028 (2018).
- [127] P. M. Ferreira, S. Liebler, and J. Wittbrodt,  $pp \rightarrow A \rightarrow Zh$  and the wrong-sign limit of the two-Higgs-doublet model, *Phys. Rev. D* **97**, 055008 (2018).
- [128] W. Su, Probing loop effects in wrong-sign Yukawa coupling region of type-II 2HDM, *Eur. Phys. J. C* **81**, 404 (2021).
- [129] X.-F. Han and H.-X. Wang, Revisiting wrong sign Yukawa coupling of type II two-Higgs-doublet model in light of recent LHC data, *Chin. Phys. C* **44**, 073101 (2020).
- [130] E. J. Chun, S. Dwivedi, T. Mondal, B. Mukhopadhyaya, and S. K. Rai, Reconstructing heavy Higgs boson masses in a type X two-Higgs-doublet model with a light pseudoscalar particle, *Phys. Rev. D* **98**, 075008 (2018).
- [131] A. Alloul, N. D. Christensen, C. Degrande, C. Duhr, and B. Fuks, FeynRules 2.0—A complete toolbox for tree-level phenomenology, *Comput. Phys. Commun.* **185**, 2250 (2014).
- [132] C. Degrande, C. Duhr, B. Fuks, D. Grellscheid, O. Mattelaer, and T. Reiter, UFO—The universal FeynRules output, *Comput. Phys. Commun.* **183**, 1201 (2012).
- [133] J. Alwall, M. Herquet, F. Maltoni, O. Mattelaer, and T. Stelzer, MadGraph 5: Going beyond, *J. High Energy Phys.* **06** (2011) 128.
- [134] R. D. Ball *et al.* (NNPDF Collaboration), Parton distributions from high-precision collider data, *Eur. Phys. J. C* **77**, 663 (2017).
- [135] A. Arbey, F. Mahmoudi, O. Stal, and T. Stefaniak, Status of the charged Higgs boson in two Higgs doublet models, *Eur. Phys. J. C* **78**, 182 (2018).
- [136] M. Misiak and M. Steinhauser, Weak radiative decays of the B meson and bounds on  $M_{H^\pm}$  in the two-Higgs-doublet model, *Eur. Phys. J. C* **77**, 201 (2017).
- [137] I. P. Ivanov, Minkowski space structure of the Higgs potential in 2HDM, *Phys. Rev. D* **75**, 035001 (2007).
- [138] A. Arhrib, Unitarity constraints on scalar parameters of the standard and two Higgs doublets model, in *Proceedings of the Workshop on Noncommutative Geometry, Superstrings and Particle Physics* (2000), [arXiv:hep-ph/0012353](https://arxiv.org/abs/hep-ph/0012353).
- [139] I. P. Ivanov, General two-order-parameter Ginzburg-Landau model with quadratic and quartic interactions, *Phys. Rev. E* **79**, 021116 (2009).
- [140] A. Barroso, P. M. Ferreira, I. P. Ivanov, R. Santos, and J. P. Silva, Evading death by vacuum, *Eur. Phys. J. C* **73**, 2537 (2013).
- [141] A. Barroso, P. M. Ferreira, I. P. Ivanov, and R. Santos, Metastability bounds on the two Higgs doublet model, *J. High Energy Phys.* **06** (2013) 045.
- [142] D. Toussaint, Renormalization effects from superheavy Higgs particles, *Phys. Rev. D* **18**, 1626 (1978).
- [143] S. Bertolini, Quantum effects in a two Higgs doublet model of the electroweak interactions, *Nucl. Phys.* **B272**, 77 (1986).
- [144] A. Pomarol and R. Vega, Constraints on  $CP$  violation in the Higgs sector from the rho parameter, *Nucl. Phys.* **B413**, 3 (1994).
- [145] M. E. Peskin and J. D. Wells, How can a heavy Higgs boson be consistent with the precision electroweak measurements?, *Phys. Rev. D* **64**, 093003 (2001).
- [146] H.-J. He, N. Polonsky, and S.-f. Su, Extra families, Higgs spectrum and oblique corrections, *Phys. Rev. D* **64**, 053004 (2001).
- [147] W. Grimus, L. Lavoura, O. M. Ogreid, and P. Osland, A precision constraint on multi-Higgs-doublet models, *J. Phys. G* **35**, 075001 (2008).
- [148] W. Grimus, L. Lavoura, O. M. Ogreid, and P. Osland, The oblique parameters in multi-Higgs-doublet models, *Nucl. Phys.* **B801**, 81 (2008).
- [149] S. Kanemura, Y. Okada, H. Taniguchi, and K. Tsumura, Indirect bounds on heavy scalar masses of the two-Higgs-doublet model in light of recent Higgs boson searches, *Phys. Lett. B* **704**, 303 (2011).
- [150] M. Aaboud *et al.* (ATLAS Collaboration), Search for Higgs bosons produced via vector-boson fusion and decaying into bottom quark pairs in  $\sqrt{s} = 13$  TeV  $pp$  collisions with the ATLAS detector, *Phys. Rev. D* **98**, 052003 (2018).
- [151] M. Aaboud *et al.* (ATLAS Collaboration), Measurements of gluon-gluon fusion and vector-boson fusion Higgs boson production cross-sections in the  $H \rightarrow WW^* \rightarrow e\nu\mu\nu$  decay channel in  $pp$  collisions at  $\sqrt{s} = 13$  TeV with the ATLAS detector, *Phys. Lett. B* **789**, 508 (2019).
- [152] M. Aaboud *et al.* (ATLAS Collaboration), Cross-section measurements of the Higgs boson decaying into a pair of  $\tau$ -leptons in proton-proton collisions at  $\sqrt{s} = 13$  TeV with the ATLAS detector, *Phys. Rev. D* **99**, 072001 (2019).
- [153] G. Aad *et al.* (ATLAS Collaboration), Higgs boson production cross-section measurements and their EFT interpretation in the  $4\ell$  decay channel at  $\sqrt{s} = 13$  TeV with the ATLAS detector, *Eur. Phys. J. C* **80**, 957 (2020).
- [154] A. M. Sirunyan *et al.* (CMS Collaboration), Search for  $t\bar{t}H$  production in the  $H \rightarrow b\bar{b}$  decay channel with leptonic  $t\bar{t}$  decays in proton-proton collisions at  $\sqrt{s} = 13$  TeV, *J. High Energy Phys.* **03** (2019) 026.
- [155] A. M. Sirunyan *et al.* (CMS Collaboration), Search for the Higgs Boson Decaying to Two Muons in Proton-Proton Collisions at  $\sqrt{s} = 13$  TeV, *Phys. Rev. Lett.* **122**, 021801 (2019).
- [156] CMS Collaboration, Measurements of properties of the Higgs boson in the four-lepton final state in proton-proton collisions at  $\sqrt{s} = 13$  TeV, Report No. CMS-PAS-HIG-19-001.

- [157] CMS Collaboration, Measurements of differential Higgs boson production cross sections in the leptonic WW decay mode at  $\sqrt{s} = 13$  TeV, Report No. CMS-PAS-HIG-19-002.
- [158] Y. S. Amhis *et al.* (HFLAV Collaboration), Averages of b-hadron, c-hadron, and  $\tau$ -lepton properties as of 2018, *Eur. Phys. J. C* **81**, 226 (2021).
- [159] L. Michel, Interaction between four half spin particles and the decay of the  $\mu$  meson, *Proc. Phys. Soc. London Sect. A* **63**, 514 (1950).
- [160] H. E. Logan and D. MacLennan, Charged Higgs phenomenology in the lepton-specific two Higgs doublet model, *Phys. Rev. D* **79**, 115022 (2009).
- [161] S. Schael *et al.* (ALEPH, DELPHI, L3, OPAL, SLD, LEP Electroweak Working Group, SLD Electroweak Group, SLD Heavy Flavour Group Collaborations), Precision electroweak measurements on the Z resonance, *Phys. Rep.* **427**, 257 (2006).
- [162] J. Oredsson and J. Rathsman,  $\mathbb{Z}_2$  breaking effects in 2-loop RG evolution of 2HDM, *J. High Energy Phys.* **02** (2019) 152.
- [163] J. Oredsson, 2HDME: Two-Higgs-doublet model evolver, *Comput. Phys. Commun.* **244**, 409 (2019).
- [164] M. Bicer *et al.* (TLEP Design Study Working Group), First look at the physics case of TLEP, *J. High Energy Phys.* **01** (2014) 164.
- [165] J. Gao, CEPC and SppC status—from the completion of CDR towards TDR, *Int. J. Mod. Phys. A* **36**, 2142005 (2021).
- [166] M. Dong *et al.* (CEPC Study Group), CEPC conceptual design report: Volume 2—physics & detector, [arXiv:1811.10545](https://arxiv.org/abs/1811.10545).
- [167] E. J. Chun and J. Kim, Leptonic precision test of leptophilic two-Higgs-doublet model, *J. High Energy Phys.* **07** (2016) 110.